OTFS: A New Modulation Scheme for 5G and Beyond

NCC'2020 Tutorial
IIT Kharagpur

A. Chockalingam
Department of ECE, IISc

Special thanks to
M. K. Ramachandran, G. D. Surabhi, Rosemary Augustine, Prof. Emanuele Viterbo

21 February 2020

Outline I

Some background

Wireless spectrum

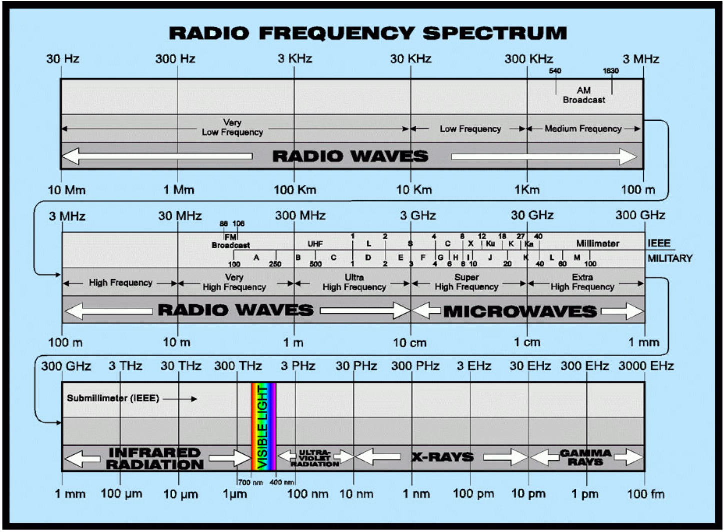

Source: Internet

Some wireless terminologies

Some wireless terminologies

- Carrier frequency (Hertz; Hz)

Some wireless terminologies

- Carrier frequency (Hertz; Hz)
- Bandwidth, W (Hz)

Some wireless terminologies

- Carrier frequency (Hertz; Hz)
- Bandwidth, W (Hz)

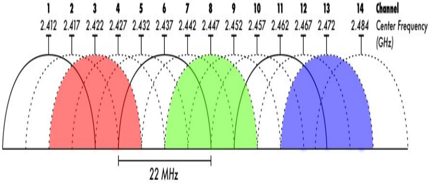

Some wireless terminologies

- Carrier frequency (Hertz; Hz)
- Bandwidth, W (Hz)

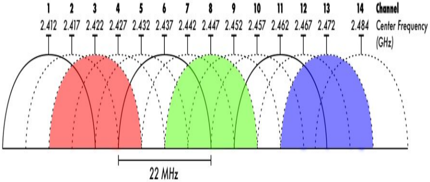

- Data rate (bits per second; bps)

Some wireless terminologies

- Carrier frequency (Hertz; Hz)
- Bandwidth, W (Hz)

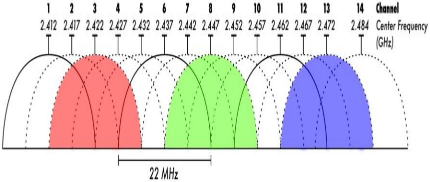

- Data rate (bits per second; bps)
- Spectral efficiency (bps per Hz; bps/Hz)

Some wireless terminologies

- Carrier frequency (Hertz; Hz)
- Bandwidth, W (Hz)

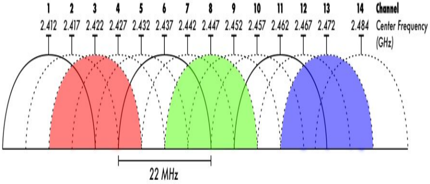

- Data rate (bits per second; bps)
- Spectral efficiency (bps per Hz; bps/Hz)
- Signaling interval, $T_s = \frac{1}{W}$ (sec)

Some wireless terminologies

- Carrier frequency (Hertz; Hz)
- Bandwidth, W (Hz)

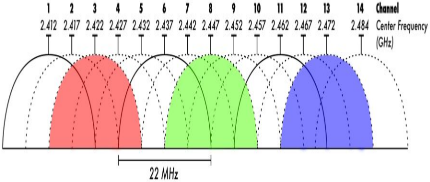

- Data rate (bits per second; bps)
- Spectral efficiency (bps per Hz; bps/Hz)
- Signaling interval, $T_s = \frac{1}{W}$ (sec)
- Signal-to-noise ratio (SNR)

Some wireless terminologies

- Carrier frequency (Hertz; Hz)
- Bandwidth, W (Hz)

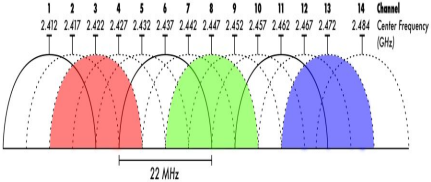

- Data rate (bits per second; bps)
- Spectral efficiency (bps per Hz; bps/Hz)
- Signaling interval, $T_s = \frac{1}{W}$ (sec)
- Signal-to-noise ratio (SNR)
- Channel capacity (bps)

Some wireless terminologies

- Carrier frequency (Hertz; Hz)
- Bandwidth, W (Hz)

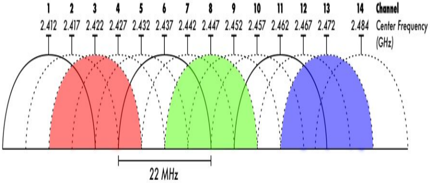

- Data rate (bits per second; bps)
- Spectral efficiency (bps per Hz; bps/Hz)
- Signaling interval, $T_s = \frac{1}{W}$ (sec)
- Signal-to-noise ratio (SNR)
- Channel capacity (bps)
- Probability of bit error

Some wireless terminologies

- Carrier frequency (Hertz; Hz)
- Bandwidth, W (Hz)

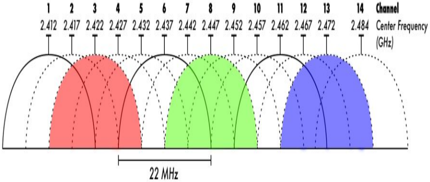

- Data rate (bits per second; bps)
- Spectral efficiency (bps per Hz; bps/Hz)
- Signaling interval, $T_s = \frac{1}{W}$ (sec)
- Signal-to-noise ratio (SNR)
- Channel capacity (bps)
- Probability of bit error
- Multipath fading

AWGN channel

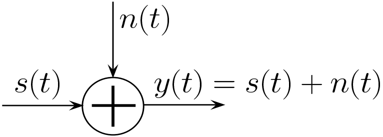

AWGN channel

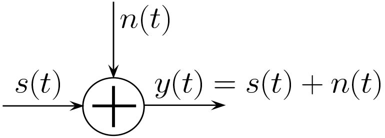

- e.g., satellite channel

AWGN channel

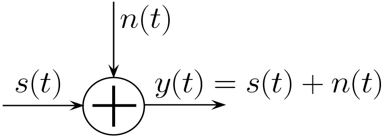

- e.g., satellite channel

Channel	Error Probability (P_e)	Capacity (C), bps
AWGN	$P_e \propto e^{-SNR}$	$C = W \log(1 + SNR)$

AWGN channel

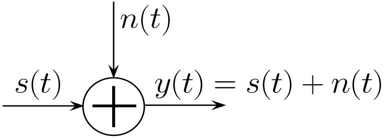

- e.g., satellite channel

Channel	Error Probability (P_e)	Capacity (C), bps
AWGN	$P_e \propto e^{-SNR}$	$C = W \log(1 + SNR)$

- Prob. of error falls exponentially with SNR

AWGN channel

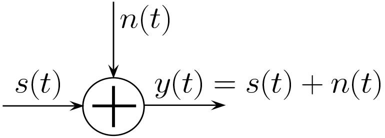

- e.g., satellite channel

Channel	Error Probability (P_e)	Capacity (C), bps
AWGN	$P_e \propto e^{-SNR}$	$C = W\ \log(1 + SNR)$

- Prob. of error falls exponentially with SNR
- Capacity grows with SNR (but only logarithmically with SNR)

Multipath fading

Multipath fading

- Fading channel characterization

Multipath fading

- Fading channel characterization
  - Variation in frequency-domain
    - Max. Delay spread (τ_{max})
    - Coherence bandwidth (W_{coh})

Multipath fading

- Fading channel characterization
  - Variation in frequency-domain
    - Max. Delay spread (τ_{max})
    - Coherence bandwidth (W_{coh})
  - Variation in time-domain
    - Max. Doppler spread (ν_{max})
    - Coherence time (T_{coh})

Multipath fading

- Variation in frequency-domain
  - Max. Delay spread (τ_{max}) and coherence bandwidth (W_{coh})

Multipath fading

- Variation in frequency-domain
  - Max. Delay spread (τ_{max}) and coherence bandwidth (W_{coh})

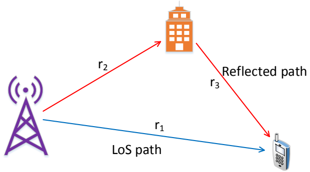

Multipath fading

- Variation in frequency-domain
  - Max. Delay spread (τ_{max}) and coherence bandwidth (W_{coh})

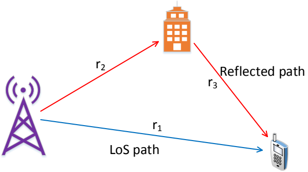

- Delay of LoS path: $\tau_1 = r_1/c$.

Multipath fading

- Variation in frequency-domain
  - Max. Delay spread (τ_{max}) and coherence bandwidth (W_{coh})

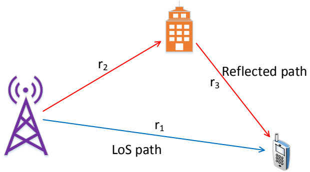

  - Delay of LoS path: $\tau_1 = r_1/c$. Delay of reflected path: $\tau_2 = (r_2 + r_3)/c$

Multipath fading

- Variation in frequency-domain
  - Max. Delay spread (τ_{max}) and coherence bandwidth (W_{coh})

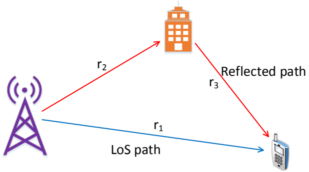

- Delay of LoS path: $\tau_1 = r_1/c$. Delay of reflected path: $\tau_2 = (r_2 + r_3)/c$
- Delay spread: $\tau_2 - \tau_1$.

Multipath fading

- Variation in frequency-domain
  - Max. Delay spread (τ_{max}) and coherence bandwidth (W_{coh})

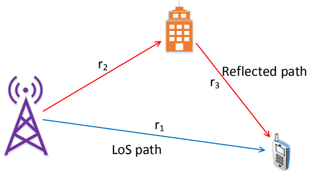

- Delay of LoS path: $\tau_1 = r_1/c$.
- Delay spread: $\tau_2 - \tau_1$.

Delay of reflected path: $\tau_2 = (r_2 + r_3)/c$

$\tau_{max} = \max_{i,j} |\tau_i - \tau_j|$

Multipath fading

- Variation in frequency-domain
  - Max. Delay spread (τ_{max}) and coherence bandwidth (W_{coh})

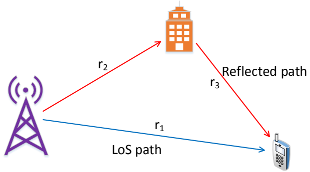

- Delay of LoS path: $\tau_1 = r_1/c$. Delay of reflected path: $\tau_2 = (r_2 + r_3)/c$
- Delay spread: $\tau_2 - \tau_1$. $\tau_{max} = \max_{i,j} |\tau_i - \tau_j|$
- $W_{coh} \propto \tau_{max}{}^{-1}$

Multipath fading

- Variation in frequency-domain
  - Max. Delay spread (τ_{max}) and coherence bandwidth (W_{coh})

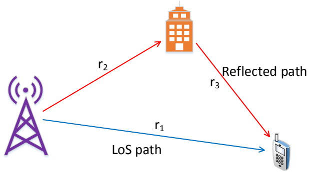

- Delay of LoS path: $\tau_1 = r_1/c$. Delay of reflected path: $\tau_2 = (r_2 + r_3)/c$
- Delay spread: $\tau_2 - \tau_1$. $\tau_{max} = \max_{i,j} |\tau_i - \tau_j|$
- $W_{coh} \propto {\tau_{max}}^{-1}$
- Frequency-flat fading: Coherence BW > Signaling BW $(W_{coh} > W)$

Multipath fading

- Variation in frequency-domain
  - Max. Delay spread (τ_{max}) and coherence bandwidth (W_{coh})

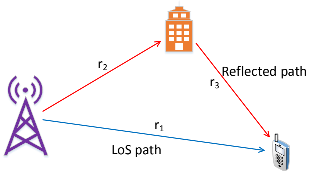

- Delay of LoS path: $\tau_1 = r_1/c$. Delay of reflected path: $\tau_2 = (r_2 + r_3)/c$
- Delay spread: $\tau_2 - \tau_1$. $\tau_{max} = \max_{i,j} |\tau_i - \tau_j|$
- $W_{coh} \propto {\tau_{max}}^{-1}$
- Frequency-flat fading: Coherence BW > Signaling BW ($W_{coh} > W$)
- Frequency-selective fading: Coherence BW < Signaling BW ($W_{coh} < W$)

Multipath fading

- Variation in frequency-domain
  - Max. Delay spread (τ_{max}) and coherence bandwidth (W_{coh})

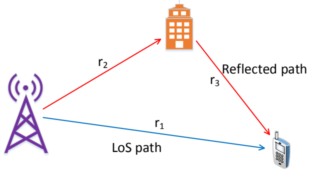

- Delay of LoS path: $\tau_1 = r_1/c$. Delay of reflected path: $\tau_2 = (r_2 + r_3)/c$
- Delay spread: $\tau_2 - \tau_1$. $\tau_{max} = \max_{i,j} |\tau_i - \tau_j|$
- $W_{coh} \propto \tau_{max}{}^{-1}$
- Frequency-flat fading: Coherence BW > Signaling BW ($W_{coh} > W$)
- Frequency-selective fading: Coherence BW < Signaling BW ($W_{coh} < W$)

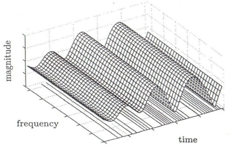

Frequency-flat fading.

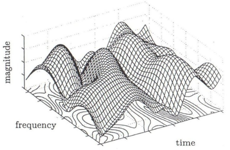

Frequency-selective fading.

Multipath fading

- Variation in time-domain
  - Max. Doppler spread (ν_{max}) and coherence time (T_{coh})

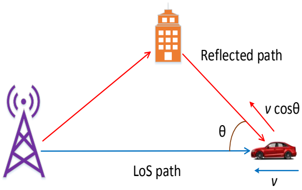

Multipath fading

- Variation in time-domain
  - Max. Doppler spread (ν_{max}) and coherence time (T_{coh})

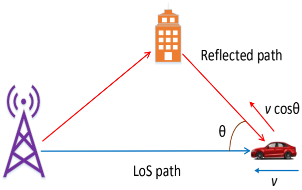

- Doppler shift of LoS path: $\nu_1 = \frac{v}{\lambda} = f_c \frac{v}{c}$

Multipath fading

- Variation in time-domain
  - Max. Doppler spread (ν_{max}) and coherence time (T_{coh})

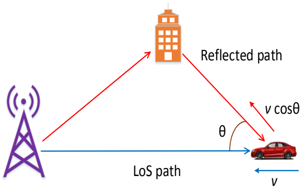

- Doppler shift of LoS path: $\nu_1 = \frac{v}{\lambda} = f_c \frac{v}{c}$
- Doppler shift of reflected path: $\nu_2 = f_c \frac{v \cos\theta}{c}$

Multipath fading

- Variation in time-domain
  - Max. Doppler spread (ν_{max}) and coherence time (T_{coh})

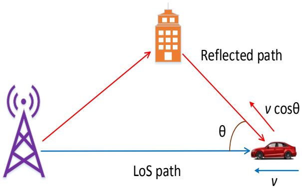

- Doppler shift of LoS path: $\nu_1 = \frac{v}{\lambda} = f_c \frac{v}{c}$
- Doppler shift of reflected path: $\nu_2 = f_c \frac{v \cos\theta}{c}$
- Doppler spread: $\nu_2 - \nu_1$

Multipath fading

- Variation in time-domain
  - Max. Doppler spread (ν_{max}) and coherence time (T_{coh})

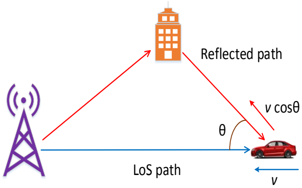

- Doppler shift of LoS path: $\nu_1 = \frac{v}{\lambda} = f_c \frac{v}{c}$
- Doppler shift of reflected path: $\nu_2 = f_c \frac{v \cos\theta}{c}$
- Doppler spread: $\nu_2 - \nu_1$ $\quad \nu_{max} = \max_{i,j} |\nu_i - \nu_j|$

Multipath fading

- Variation in time-domain
  - Max. Doppler spread (ν_{max}) and coherence time (T_{coh})

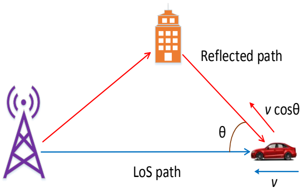

- Doppler shift of LoS path: $\nu_1 = \frac{v}{\lambda} = f_c \frac{v}{c}$
- Doppler shift of reflected path: $\nu_2 = f_c \frac{v \cos\theta}{c}$
- Doppler spread: $\nu_2 - \nu_1$ $\quad \nu_{max} = \max_{i,j} |\nu_i - \nu_j|$

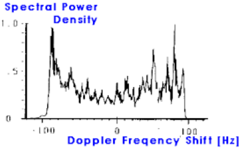

Multipath fading

- Variation in time-domain
  - Max. Doppler spread (ν_{max}) and coherence time (T_{coh})

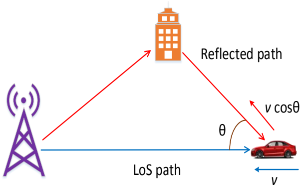

- Doppler shift of LoS path: $\nu_1 = \frac{v}{\lambda} = f_c \frac{v}{c}$
- Doppler shift of reflected path: $\nu_2 = f_c \frac{v \cos\theta}{c}$
- Doppler spread: $\nu_2 - \nu_1$ $\quad \nu_{max} = \max_{i,j} |\nu_i - \nu_j|$

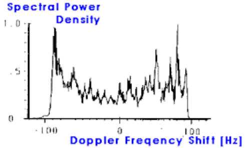

- $T_{coh} \propto \nu_{max}{}^{-1}$

Multipath fading

- Variation in time-domain
  - Max. Doppler spread (ν_{max}) and coherence time (T_{coh})

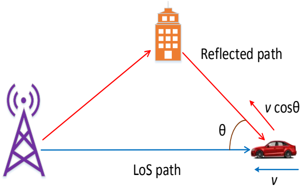

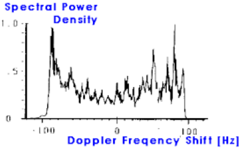

- Doppler shift of LoS path: $\nu_1 = \frac{v}{\lambda} = f_c \frac{v}{c}$
- Doppler shift of reflected path: $\nu_2 = f_c \frac{v \cos\theta}{c}$
- Doppler spread: $\nu_2 - \nu_1$ $\quad \nu_{max} = \max_{i,j} |\nu_i - \nu_j|$

- $T_{coh} \propto {\nu_{max}}^{-1}$
- Slow fading: Coherence time > signaling interval ($T_{coh} > T_s$)

Multipath fading

- Variation in time-domain
  - Max. Doppler spread (ν_{max}) and coherence time (T_{coh})

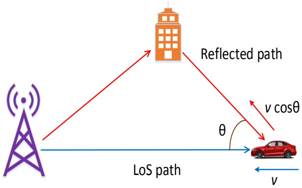

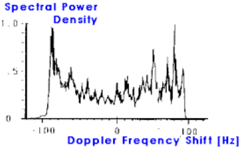

- Doppler shift of LoS path: $\nu_1 = \frac{v}{\lambda} = f_c \frac{v}{c}$
- Doppler shift of reflected path: $\nu_2 = f_c \frac{v\cos\theta}{c}$
- Doppler spread: $\nu_2 - \nu_1$ $\quad \nu_{max} = \max_{i,j} |\nu_i - \nu_j|$

- $T_{coh} \propto {\nu_{max}}^{-1}$
- Slow fading: Coherence time > signaling interval ($T_{coh} > T_s$)
- Fast fading: Coherence time < signaling interval ($T_{coh} < T_s$)

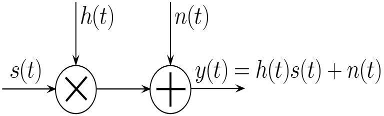

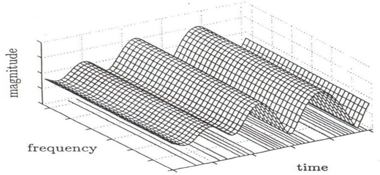

Frequency-flat fading.

- e.g., mobile radio channel

Channel	Error Probability (P_e)	Capacity (C), bps
Fading	$P_e \propto SNR^{-1}$	$C = W \log(1 + SNR)$

- Prob. of error falls only linearly with SNR

Prob. of bit error performance

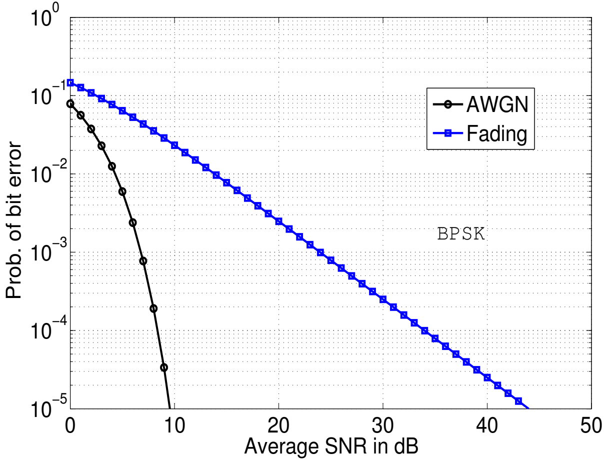

ISI channel

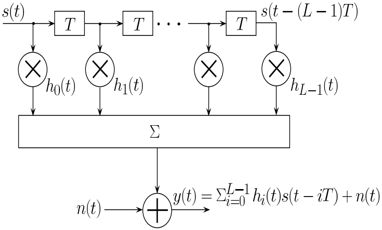

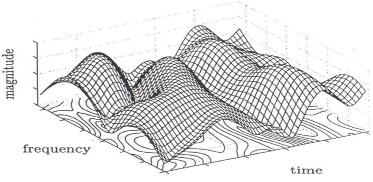

Frequency-selective fading.

- e.g., mobile radio channel

Channel	Error Probability (P_e)	Capacity (C), bps
ISI	$P_e \propto SNR^{-L}$	$C = W \log(1 + SNR)$

- Causes inter-symbol interference (ISI)
- If rx. signal is properly processed (equalization)
  - prob. of error falls with Lth power of SNR (multipath diversity)

OFDM in ISI channels

- Orthogonal Frequency Division Multiplexing (overcomes ISI issue)

OFDM in ISI channels

- Orthogonal Frequency Division Multiplexing (overcomes ISI issue)
  - Converts frequency-selective channel to multiple (M) frequency-flat channels

OFDM in ISI channels

- Orthogonal Frequency Division Multiplexing (overcomes ISI issue)
    - Converts frequency-selective channel to multiple (M) frequency-flat channels

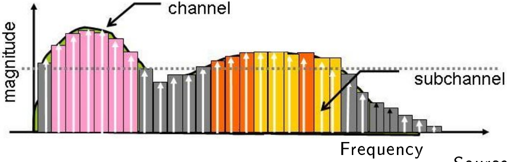

Source: Internet

OFDM in ISI channels

- Orthogonal Frequency Division Multiplexing (overcomes ISI issue)
  - Converts frequency-selective channel to multiple (M) frequency-flat channels

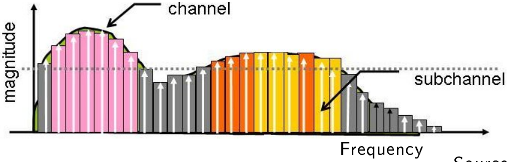

Source: Internet

  - Multiplexes M information symbols $X(k), k = 0, \cdots, M-1$ on M subcarriers

OFDM in ISI channels

- Orthogonal Frequency Division Multiplexing (overcomes ISI issue)
  - Converts frequency-selective channel to multiple (M) frequency-flat channels

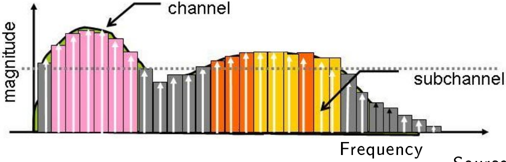

Source: Internet

  - Multiplexes M information symbols $X(k), k = 0, \cdots, M-1$ on M subcarriers

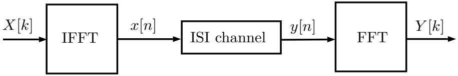

OFDM in ISI channels

- Orthogonal Frequency Division Multiplexing (overcomes ISI issue)
  - Converts frequency-selective channel to multiple (M) frequency-flat channels

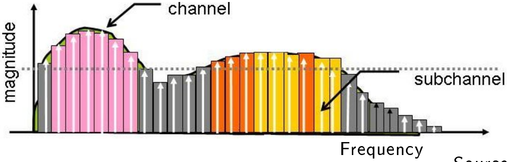

Source: Internet

  - Multiplexes M information symbols $X(k), k = 0, \cdots, M-1$ on M subcarriers

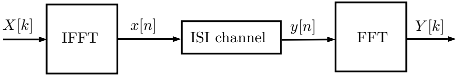

- Tx: $x(n) = \frac{1}{\sqrt{M}} \sum_{k=0}^{M-1} X(k) e^{\frac{j2\pi kn}{M}}, \; n = 0, 1, \cdots, M-1$

OFDM in ISI channels

- Orthogonal Frequency Division Multiplexing (overcomes ISI issue)
  - Converts frequency-selective channel to multiple (M) frequency-flat channels

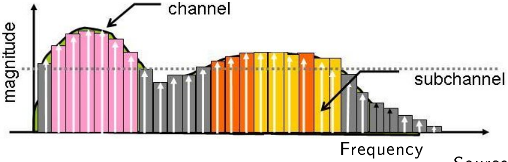

Source: Internet

  - Multiplexes M information symbols $X(k), k = 0, \cdots, M-1$ on M subcarriers

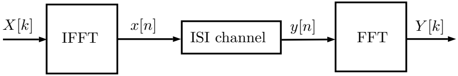

  - Tx: $x(n) = \frac{1}{\sqrt{M}} \sum_{k=0}^{M-1} X(k) e^{\frac{j2\pi kn}{M}}, \; n = 0, 1, \cdots, M-1$
  - Rx: $Y(k) = \frac{1}{\sqrt{M}} \sum_{n=0}^{M-1} y(n) e^{\frac{-j2\pi kn}{M}}, \; k = 0, 1, \cdots, M-1$

OFDM in ISI channels

- Orthogonal Frequency Division Multiplexing (overcomes ISI issue)
  - Converts frequency-selective channel to multiple (M) frequency-flat channels

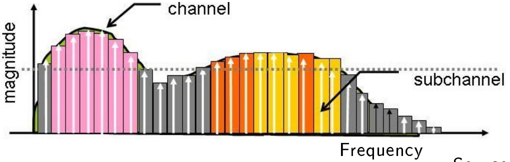

Source: Internet

  - Multiplexes M information symbols $X(k), k = 0, \cdots, M-1$ on M subcarriers

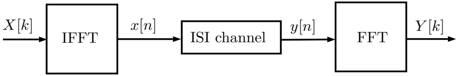

  - Tx: $x(n) = \frac{1}{\sqrt{M}} \sum_{k=0}^{M-1} X(k) e^{\frac{j2\pi kn}{M}}, \; n = 0, 1, \cdots, M-1$
  - Rx: $Y(k) = \frac{1}{\sqrt{M}} \sum_{n=0}^{M-1} y(n) e^{\frac{-j2\pi kn}{M}}, \; k = 0, 1, \cdots, M-1$
  - Renders the ISI channel to a multiplicative channel, $Y(k) = H(k)X(k) + N(k)$

SIMO channel

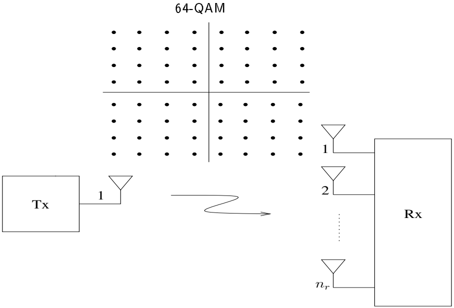

- e.g., mobile radio channel

Channel	Error Probability (P_e)	Capacity (C), bps
SIMO	$P_e \propto SNR^{-n_r}$	$C = W \log(1 + SNR)$

- Prob. of error falls with n_rth power of SNR (receive diversity)

MIMO channel

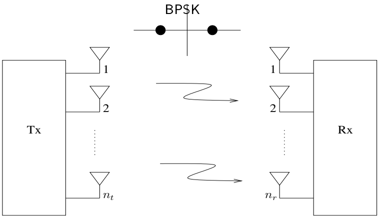

- e.g., mobile radio channel $\mathbf{y} = \mathbf{H}\mathbf{x} + \mathbf{n}$

Channel	Error Probability (P_e)	Capacity (C), bps
MIMO	$P_e \propto SNR^{-n_t n_r}$	$C = \min(n_t, n_r) W \log(1 + SNR)$

- Prob. of error falls with $n_t n_r$th power of SNR (tx & rx diversity)
- Capacity grows linearly with n_t, n_r
- Large n_t, n_r $\Longrightarrow$ large capacity/diversity gains (massive MIMO in 5G)
- MIMO signal detection problem: $\hat{\mathbf{x}} = \arg\max_{\mathbf{x} \in \mathbb{A}^{n_t}} \|\mathbf{y} - \mathbf{H}\mathbf{x}\|^2$

Prob. of bit error performance

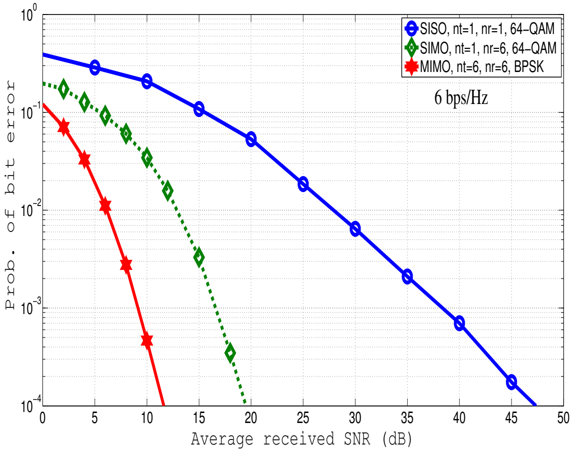

- MIMO
  - spectrally efficient, reliable, power efficient

Multiuser communication

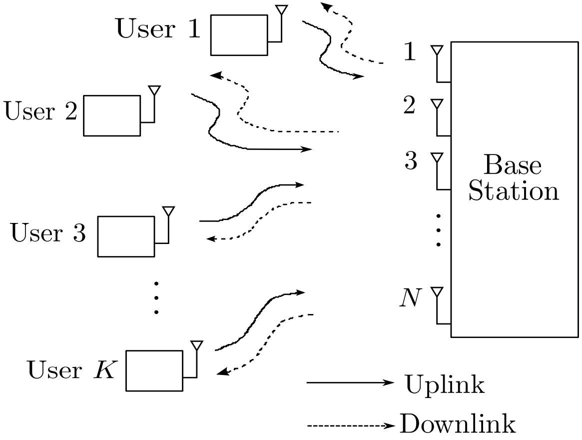

Cellular wireless evolution

Generation	Frequency band	PHY features	Data rate	Spectral Eff. (bps/Hz)
1G	850 MHz	FDMA, FM	N/A	N/A
2G	900 MHz, 1.8 GHz	TDMA/CDMA, GMSK/QPSK, FEC, PC	10 Kbps	< 1
3G	1.8–2.5 GHz	CDMA, QAM	1–40 Mbps	1–8
4G	2–8 GHz	OFDMA, SC-FDMA QAM, MIMO-OFDM	100–600 Mbps	15
5G	1–6 GHz mm wave (26-28 GHz) $<$ 1 GHz (massive IoT) visible light?	massive MIMO beamforming D2D, Full duplex, NOMA LDPC and Polar codes OFDM & variants (adapted to extremes?)	multi-Gbps	several tens

- Waveform design is the major change between the generations

High-mobility requirement in 5G

5G vision

1. Enhanced mobile broadband (eMBB) [2020-2021] (user focus)
   - High data rates (multi-gigabits per sec)
   - High spectral efficiency (tens of bps/Hz)
   - High capacity (10 Tbps per Km^2)
   - High user mobility?

5G vision

1. Enhanced mobile broadband (eMBB) [2020-2021] (user focus)
   - High data rates (multi-gigabits per sec)
   - High spectral efficiency (tens of bps/Hz)
   - High capacity (10 Tbps per Km^2)
   - High user mobility?
2. Massive machine type communications (mMTC) [2021-2022] (device focus)
   - Massive Internet of Things
   - High density (1 million nodes per Km^2)
   - Ultra-low energy (10 years+ battery life)
   - Deep coverage (reach challenging locations)

5G vision

1. Enhanced mobile broadband (eMBB) [2020-2021] (user focus)
   - High data rates (multi-gigabits per sec)
   - High spectral efficiency (tens of bps/Hz)
   - High capacity (10 Tbps per Km^2)
   - High user mobility?
2. Massive machine type communications (mMTC) [2021-2022] (device focus)
   - Massive Internet of Things
   - High density (1 million nodes per Km^2)
   - Ultra-low energy (10 years+ battery life)
   - Deep coverage (reach challenging locations)
3. Ultra-reliable and low-latency communications (uRLLC) [2024-2025]
   - Mission-critical services
   - Ultra-low latency ($<$ 1 msec end-to-end latency)
   - Ultra-high reliability ($<$ 1 out of 100 million packets lost)
   - Strong security (health/financial/government)

High-mobility support

- Mobility support requirement
  - relative speed between the user and the network edge at which consistent user experience must be ensured
- Enhanced mobility support ($\sim$ 5-fold) compared to that in 4G
- Mobility on demand
  - ranging from very high mobility users (e.g., users in bullet trains, airplanes) to low mobility/stationary devices (e.g., smart meters)

Scenario	User experienced data rate	E2E latency	Mobility
Mobile BB in vehicles (cars, trains)	DL: 50 Mbps UL: 25 Mbps	10 msec	on demand up to 500 km/h
Airplane connectivity	DL: 15 Mbps UL: 7.5 Mbps	10 msec	on demand up to 1000 km/h

Scenario	Connection density	Traffic density
Mobile BB in vehicles (cars, trains)	2000/km^2 500 active users/train, 4 trains or 1 active user/car, 2000 cars	DL: 100 Gbps/km^2 (25 Gbps/train, 50 Mbps/car) UL: 50 Gbps/km^2 (12.5 Gbps/train, 25 Mbps/car)
Airplane connectivity	80/plane 60 airplanes/18000 km^2	DL: 1.2 Gbps/plane 600 Mbps/plane

(*) "5G White Paper," ver 1.0, NGMN Alliance, Feb. 2015.

High-Doppler wireless channels

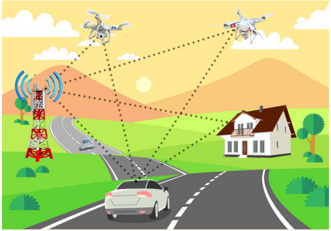

- High Dopplers due to
  - High mobility (e.g., bullet trains)

Carrier frequency	UE speed	Doppler shift
4 GHz	27 kmph	100 Hz
	100 kmph	370.3 Hz
	500 kmph	1.851 KHz

  - High carrier frequencies (e.g., mmWave, 28 GHz)

Carrier frequency	UE speed	Doppler shift
28 GHz	27 kmph	700 Hz
	54 kmph	1.4 KHz

OFDM (Modulation in 4G)

- OFDM
  - Information is signaled in the frequency domain
  - 1-D transform in frequency domain (IFFT/FFT)
  - Orthogonality among the subcarriers is the key

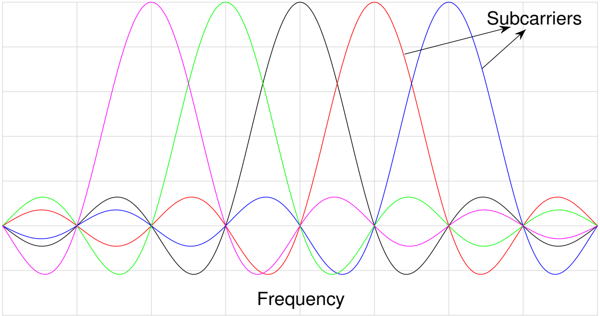

Effect of high Doppler in OFDM

- In presence of high Doppler, subcarriers lose orthogonality
- This results in inter-carrier interference (ICI)

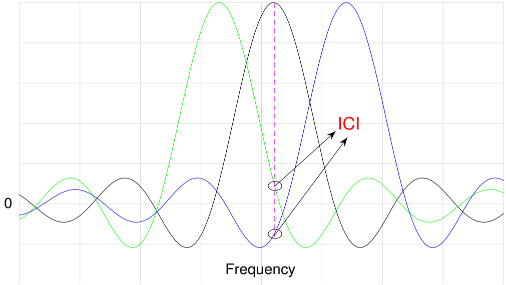

- Causes severe degradation in bit error performance for high Dopplers (error floors)
- Channel estimation and equalization in high Doppler channels is difficult

Time-frequency modulation

Time-frequency modulation

- Bin both frequency and time axes (motivation: overcome the ICI effect)

- Bin both frequency and time axes (motivation: overcome the ICI effect)
- M frequency bins and N time bins

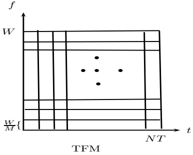

Time-frequency modulation

- Bin both frequency and time axes (motivation: overcome the ICI effect)
- M frequency bins and N time bins

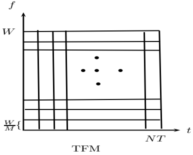

- Multiplex MN information symbols, $X(n,m)$, in the TF grid

Time-frequency modulation

- Bin both frequency and time axes (motivation: overcome the ICI effect)
- M frequency bins and N time bins

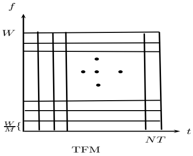

- Multiplex MN information symbols, $X(n,m)$, in the TF grid

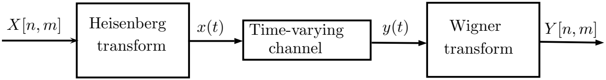

Time-frequency modulation

- Bin both frequency and time axes (motivation: overcome the ICI effect)
- M frequency bins and N time bins

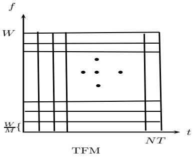

- Multiplex MN information symbols, $X(n, m)$, in the TF grid

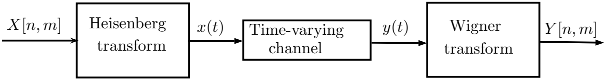

- Perform 2-D transform in the TF plane

Time-frequency modulation

- Bin both frequency and time axes (motivation: overcome the ICI effect)
- M frequency bins and N time bins

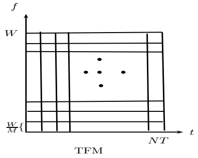

- Multiplex MN information symbols, $X(n,m)$, in the TF grid

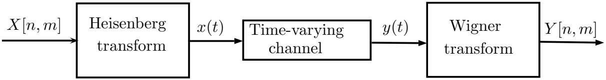

- Perform 2-D transform in the TF plane
- Tx: $x(t) = \sum_{n=0}^{N-1} \sum_{m=0}^{M-1} X[n,m] g_t(t-nT) e^{j2\pi m\Delta f(t-nT)}$

Time-frequency modulation

- Bin both frequency and time axes (motivation: overcome the ICI effect)
- M frequency bins and N time bins

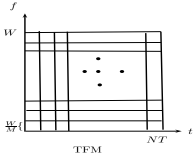

- Multiplex MN information symbols, $X(n, m)$, in the TF grid

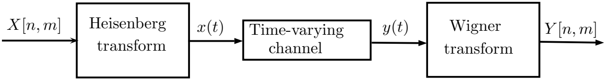

- Perform 2-D transform in the TF plane
- Tx: $x(t) = \sum_{n=0}^{N-1} \sum_{m=0}^{M-1} X[n, m] g_t(t - nT) e^{j2\pi m\Delta f(t-nT)}$
- Rx: $Y[n, m] = A(t, f)|_{t=nT, f=m\Delta f}$, $A(t, f) = \int y(t') g_r^*(t' - t) e^{-j2\pi f(t'-t)} dt'$

Time-frequency modulation

- Bin both frequency and time axes (motivation: overcome the ICI effect)
- M frequency bins and N time bins

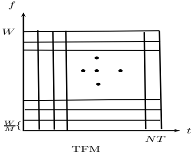

- Multiplex MN information symbols, $X(n, m)$, in the TF grid

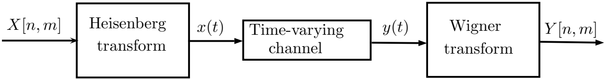

- Perform 2-D transform in the TF plane
- Tx: $x(t) = \sum_{n=0}^{N-1} \sum_{m=0}^{M-1} X[n,m] g_t(t - nT) e^{j2\pi m\Delta f(t-nT)}$
- Rx: $Y[n,m] = A(t,f)|_{t=nT, f=m\Delta f}$, $A(t,f) = \int y(t') g_r^*(t'-t) e^{-j2\pi f(t'-t)} dt'$
- $Y[n,m] = H[n,m]X[n,m] + v[n,m]$

Time-frequency modulation

- Bin both frequency and time axes (motivation: overcome the ICI effect)
- M frequency bins and N time bins

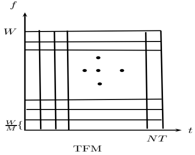

- Multiplex MN information symbols, $X(n,m)$, in the TF grid

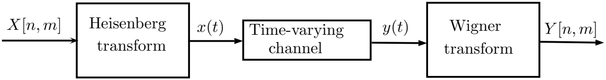

- Perform 2-D transform in the TF plane
- Tx: $x(t) = \sum_{n=0}^{N-1} \sum_{m=0}^{M-1} X[n,m] g_t(t-nT) e^{j2\pi m \Delta f (t-nT)}$
- Rx: $Y[n,m] = A(t,f)|_{t=nT, f=m\Delta f}$, $A(t,f) = \int y(t') g_r^*(t'-t) e^{-j2\pi f(t'-t)} dt'$
- $Y[n,m] = H[n,m] X[n,m] + v[n,m]$
- Do not perform that well in high Dopplers

OTFS modulation

Orthogonal Time Frequency Space (OTFS) modulation*

- A promising modulation scheme for doubly-selective channels
- Information is signaled in Delay-Doppler (DD) domain rather than in Time-Frequency (TF) domain

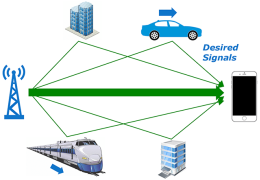

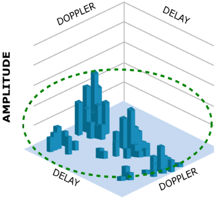

(*) R. Hadani, S. Rakib, M. Tsatsanis, A. Monk, A. J. Goldsmith, A. F. Molisch, and R. Calderbank, "Orthogonal time frequency space modulation," in *Proc. IEEE WCNC*, San Francisco, CA, USA, March 2017.

Why OTFS?

- OTFS Vs OFDM: A performance comparison

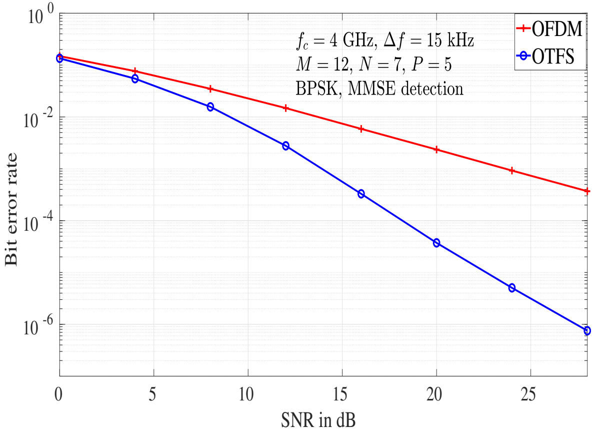

Figure : BER comparison of OTFS and OFDM systems with MMSE detection for $f_c = 4$ GHz, $\Delta f = 15$ KHz, $M = 12$, $N = 7$, $P = 5$, $\nu_{max} = 1.85$ KHz, BPSK.

Key features of OTFS

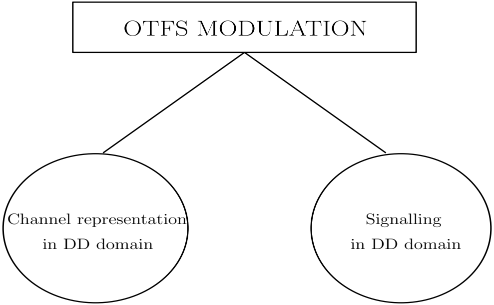

- Channel response in DD domain is invariant (for a larger observation time than in TF representation) and compact
- Each symbol experiences nearly constant channel gain
- Converts the multiplicative action of channel into a 2D convolution interaction with transmitted symbols

Channel representation in DD domain

- Different representations can be used to model LTV multipath channel
  - in time (t), frequency (f), delay (τ), and Doppler (ν) variables
- Impulse response of a time-varying channel can be expressed as a function of
  - time-frequency $H(t, f)$
  - time-delay $g(t, \tau)$
  - delay-Doppler $h(\tau, \nu)$

Channel representation in DD domain

- Different representations can be used to model LTV multipath channel
  - in time (t), frequency (f), delay (τ), and Doppler (ν) variables
- Impulse response of a time-varying channel can be expressed as a function of
  - time-frequency $H(t, f)$
  - time-delay $g(t, \tau)$
  - delay-Doppler $h(\tau, \nu)$

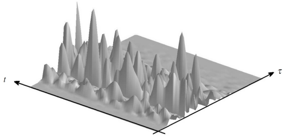

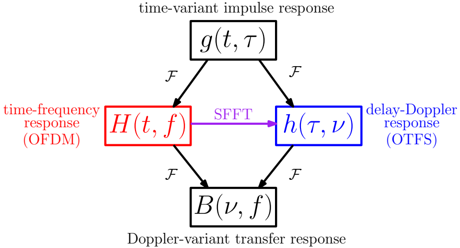

Channel representation in DD domain

- Different representations can be used to model LTV multipath channel
  - in time (t), frequency (f), delay (τ), and Doppler (ν) variables
- Impulse response of a time-varying channel can be expressed as a function of
  - time-frequency $H(t, f)$
  - time-delay $g(t, \tau)$
  - delay-Doppler $h(\tau, \nu)$

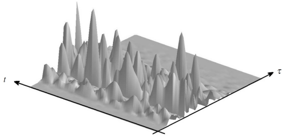

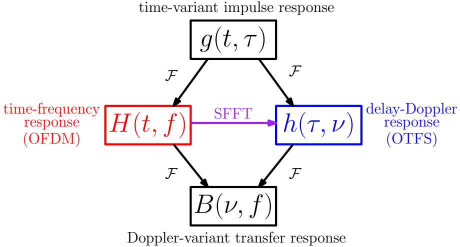

- In time-frequency $H(t, f)$ and time-delay $h(t, \tau)$ representations
  - channel coefficients vary with time at a rate that depends on mobility and carrier frequency

Time-frequency and delay-Doppler responses

- DD domain impulse response $h(\tau, \nu)$ is more compact
  - channel taps in DD representation correspond to a cluster of reflectors with specific delay and Doppler values
  - the delay and Doppler values depend on reflectors' relative distance and relative velocity, respectively, with the transmitter and receiver
  - relative velocity and distance remain roughly constant for at least a few msecs
  - Hence channel in DD domain appears time invariant for a longer duration
  - DD representation results in a sparse representation

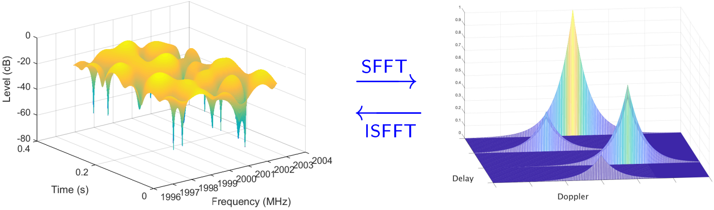

Channel in time-frequency $H(t, f)$ and delay-Doppler $h(\tau, \nu)$ domains

An example: Urban multi-lane scenario

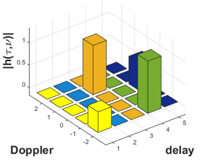

time $t = t_0$

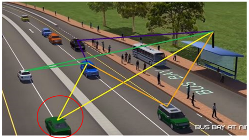

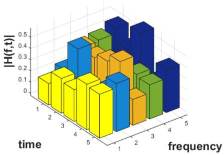

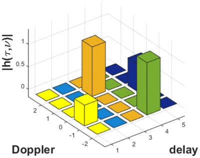

time $t = t_0 + \Delta$

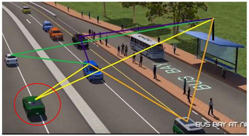

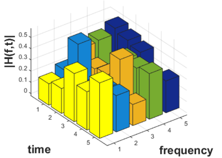

Example of a wireless channel in an urban multi-lane scenario illustrating the sparsity and slow variability of the channel in the DD representation.

$$y(t) = \int_{\nu}\int_{\tau} h(\tau,\nu)x(t-\tau)e^{j2\pi\nu(t-\tau)}\mathrm{d}\tau\mathrm{d}\nu + v(t), \quad h(\tau,\nu) = \sum_{i=1}^{P} h_i\delta(\tau-\tau_i)\delta(\nu-\nu_i), P = 4$$

Signal representation in delay-Doppler domain

- A signal can be represented as a function of time, or as a function of frequency, or as a quasi-periodic function of delay and Doppler
- These 3 representations are interchangeable by means of canonical transforms

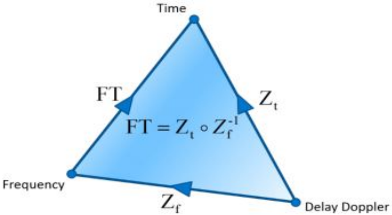

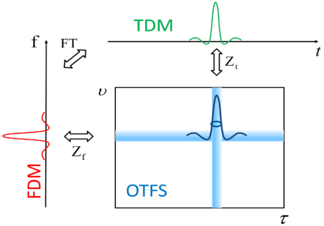

$$Z_t(\phi) = \int_0^{\nu_r} e^{j2\pi t\nu}\phi(t,\nu)\mathrm{d}\nu$$

$$Z_f(\phi) = \int_0^{\tau_r} e^{-j2\pi\tau f}\phi(\tau,f)\mathrm{d}\tau$$

- Using Zak transforms $Z_t(\phi)$ and $Z_f(\phi)$, symbols in DD domain can be converted into time and frequency domains

OTFS block diagram

- Two-step transform: DD domain → TF domain → time domain
- Implemented using simple pre- and post-processing (ISFFT & SFFT) over any multicarrier modulation scheme such as OFDM.

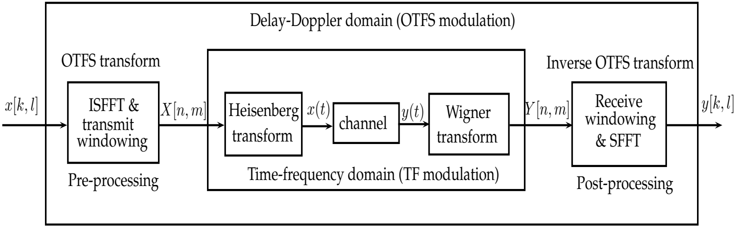

Figure : OTFS block diagram

Signaling in delay-Doppler domain

- The information symbols in DD domain $x[k,l]$s are mapped to TF symbols $X[n,m]$ using ISFFT as

$$X[n,m] = \frac{1}{\sqrt{MN}} \sum_{k=0}^{N-1} \sum_{l=0}^{M-1} x[k,l] e^{j2\pi\left(\frac{nk}{N} - \frac{ml}{M}\right)}$$

- TF plane is sampled at intervals T and Δf, to obtain a 2D grid

$$\Lambda = \{(nT, m\Delta f), n = 0, \cdots, N-1, m = 0, \cdots, M-1\}$$

- Delay-Doppler grid Γ, reciprocal to Λ

$$\Gamma = \{(\frac{k}{NT}, \frac{l}{M\Delta f}), k = 0, \cdots, N-1, l = 0, \cdots, M-1\}$$

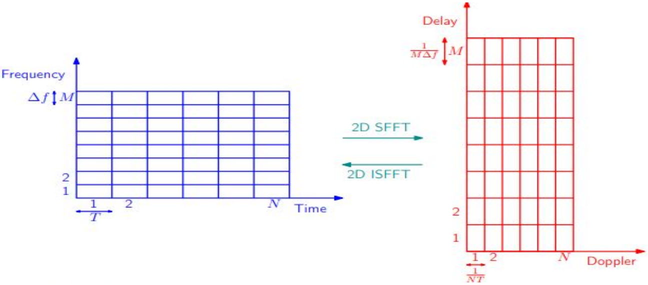

Signaling in delay-Doppler domain

- A 2D ISFFT translates every point on the DD plane into a corresponding basis function that covers the entire TF plane (2D orthogonal complex exponentials)

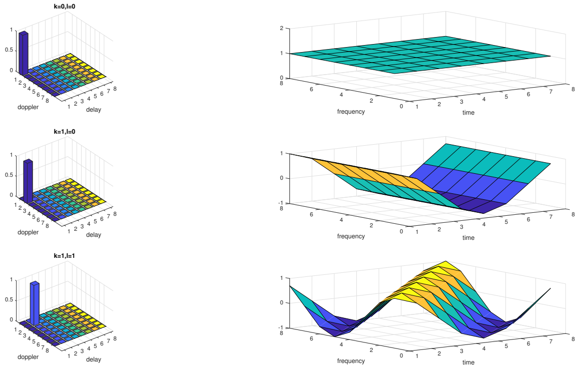

- OTFS basis functions (waveforms) have strong resilience to delay-Doppler shifts imparted by the channel (2D localized pulses in the DD domain)

OTFS basis functions

- $M = N = 32$, $\Delta f = 15$ KHz

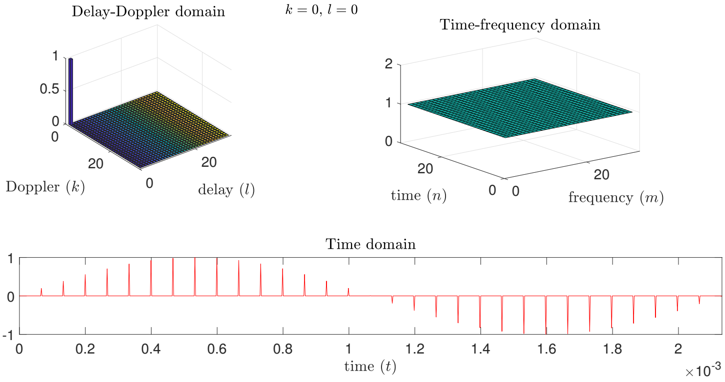

Figure : OTFS basis functions in delay-Doppler domain, time-frequency domain, and time domain for Doppler index $k = 0$ and delay index $l = 0$.

OTFS basis functions

- $M = N = 32$, $\Delta f = 15$ KHz

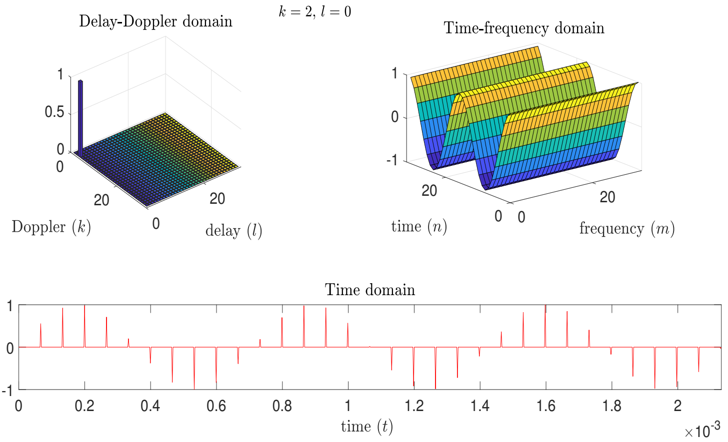

Figure : OTFS basis functions in delay-Doppler domain, time-frequency domain, and time domain for Doppler index $k = 2$ and delay index $l = 0$.

OTFS basis functions

- $M = N = 32$, $\Delta f = 15$ KHz

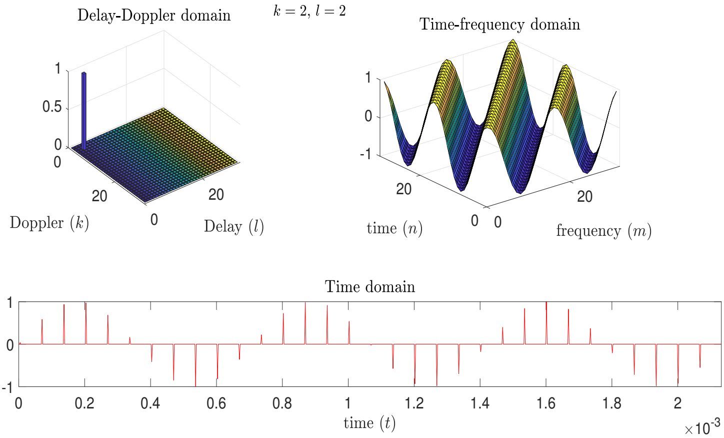

Figure : OTFS basis functions in delay-Doppler domain, time-frequency domain, and time domain for Doppler index $k = 2$ and delay index $l = 2$.

OTFS basis functions

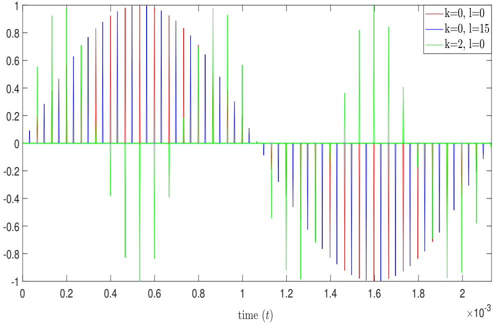

Figure : OTFS basis functions in time domain for $(k, l) = (0, 0)$, $(k, l) = (0, 15)$, and $(k, l) = (2, 0)$.

- as Doppler index (k) changes, frequency of pulse train changes (as in FDM)
- as delay index (l) changes, position of pulses gets shifted in time (as in TDM)

Time-frequency domain (inner block)

- Modulator: Heisenberg transform

$$x(t) = \sum_{n=0}^{N-1} \sum_{m=0}^{M-1} X[n,m] g_{tx}(t - nT) e^{j2\pi m\Delta f(t-nT)}$$

- Channel: $h(\tau, \nu)$

$$y(t) = \int_{\nu} \int_{\tau} h(\tau,\nu) x(t-\tau) e^{j2\pi\nu(t-\tau)} \mathrm{d}\tau \mathrm{d}\nu + v(t)$$

- Demodulator: Wigner Transform

$$Y(t,f) = A_{g_{rx},y}(t,f) = \int g_{rx}^{*}(t' - t) y(t') e^{-j2\pi\nu(t'-t)} \mathrm{d}t'$$

$$Y[n,m] = A_{g_{rx},y}(t,f)|_{t=nT, f=m\Delta f}$$

Back to delay-Doppler domain

- If $h(\tau,\nu)$ is bounded by $(\tau_{\max},\nu_{\max})$ s.t $\nu_{\max} < \Delta f < 1/\tau_{\max}$, and $g_{tx}(t)$ and $g_{rx}(t)$ satisfy the bi-orthogonality robustness condition[1], then[1]

$$Y[n,m] = H[n,m]X[n,m] + V[n,m],$$

$$H[n,m] = \int_{\tau}\int_{\nu} h(\tau,\nu)e^{j2\pi\nu nT}e^{-j2\pi(\nu+m\Delta f)\tau}\mathrm{d}\nu\mathrm{d}\tau$$

- SFFT is then applied to $Y[n,m]$ to convert it back to delay-Doppler domain to obtain $y[k,l]$ as

$$y[k,l] = \frac{1}{\sqrt{MN}}\sum_{n=0}^{N-1}\sum_{m=0}^{M-1} Y[n,m]e^{-j2\pi\left(\frac{nk}{N}-\frac{ml}{M}\right)}$$

---

[1] P. Raviteja, K. T. Phan, and E. Viterbo, "Interference cancellation and iterative detection for orthogonal time frequency space modulation," *IEEE Trans. Wireless Commun.*, vol. 17, no. 10, pp. 6501-6515, Oct. 2018.

Input-output relation

- For a channel with P paths in the delay-Doppler domain

$$h(\tau,\nu)=\sum_{i=1}^{P} h_i\delta(\tau-\tau_i)\delta(\nu-\nu_i)$$

- Received signal in delay-Doppler domain: $\tau_i \triangleq \frac{\alpha_i}{M\Delta f}$ and $\nu_i \triangleq \frac{\beta_i}{NT}$

$$y[k,l]=\sum^{P} h_i e^{-j2\pi\nu_i\tau_i} x[(k-\beta_i)_N,(l-\alpha_i)_M]+v[k,l]$$ (2D Circular Convolution)

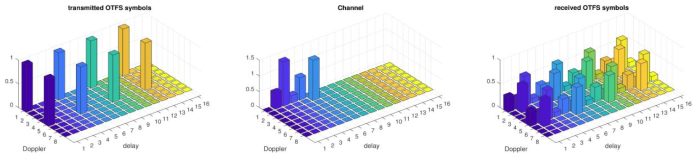

- Vectorized formulation: Input-output relation can be vectorized as

$$\mathbf{y}=\mathbf{H}\mathbf{x}+\mathbf{v},$$

where $\mathbf{x},\mathbf{y},\mathbf{v}\in\mathbb{C}^{MN\times 1}$, $\mathbf{H}\in\mathbb{C}^{MN\times MN}$, $x_{k+Nl}=x[k,l]$

- $\mathbf{H}$ is a block circulant matrix with circulant blocks, with each row having P non-zero elements

Performance of OTFS

OTFS performance

- Simulation parameters I

Parameter	**Value**
Carrier frequency (GHz)	4
Subcarrier spacing (kHz)	15
Frame size (M, N)	$(12, 7)$
Number of paths (P)	5
Delay profile	Exponential power-delay profile
Maximum speed (km/h)	500
Modulation scheme	BPSK

- Smallest resource block used in LTE: $M = 12,\ N = 7$

OTFS performance

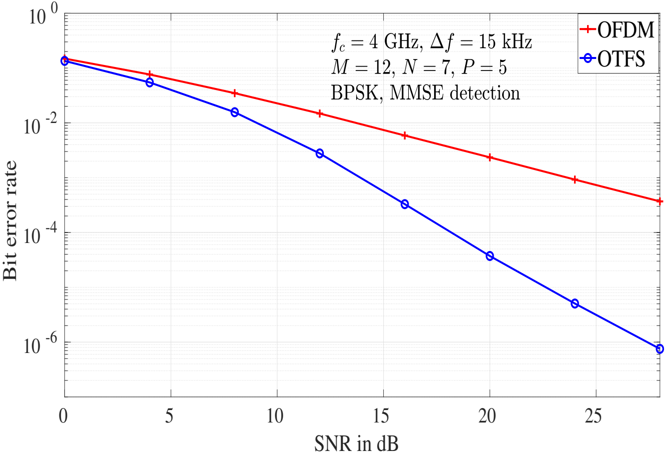

Figure : Performance of OTFS and OFDM

OTFS performance

- Simulation parameters II: IEEE 802.11p (WAVE)

Parameter	**Value**
Carrier frequency (GHz)	5.9
Subcarrier spacing (MHz)	0.156
Frame size (M, N)	$(64, 12)$
Number of paths (P)	8
Delay profile	Exponential power-delay profile
Maximum speed (km/h)	220
Modulation scheme	BPSK

OTFS performance

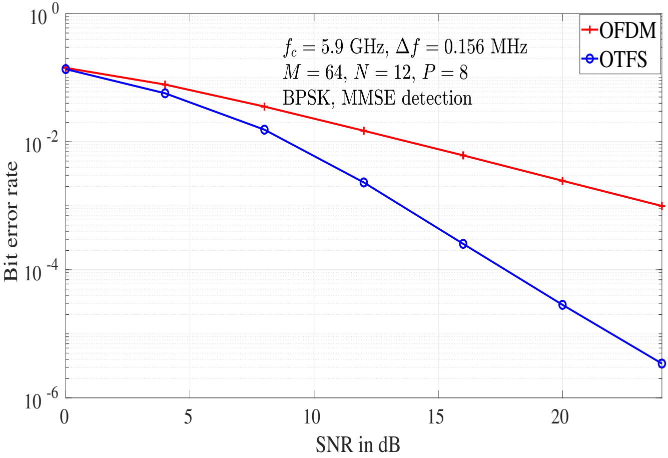

Figure : Performance of OTFS and OFDM

Choice of M & N

Choice of M & N

- M decides the delay resolution and $\nu_{\max} < \frac{W}{M} = \Delta f < 1/\tau_{\max}$
- N decides Doppler resolution and latency ($T_l = NT$)

- Example: For $\tau_{\max} = 1\ \mu$s, $\nu_{\max} = 5$ kHz, $W = 10$ MHz, and $T_l = 1$ ms,
  - $\nu_{\max} < \Delta f < 1/\tau_{\max} \implies 5$ KHz $< \Delta f < 1$ MHz
  - Δf can be chosen to be 20 kHz ($\implies M = \frac{10\times10^6}{20\times10^3} = 500$)
  - $T_l = NT = MNT_s = \frac{MN}{W} = \frac{MN}{M\Delta f} = \frac{N}{\Delta f}$

    $\implies N = T_l\Delta f = 1 \times 10^{-3} \times 20 \times 10^3 = 20$
  - (M, N) can be chosen as (500,20)

Diversity in OTFS

Diversity performance of OTFS

- There are only P non-zero elements in each row and column of the equivalent channel matrix ($\mathbf{H}$)
- Input-output relation can be rewritten in an alternate form as

$$\mathbf{y}^T = \mathbf{h}'\mathbf{X} + \mathbf{v}^T,$$

where $\mathbf{h}'$ is a $1 \times P$ vector whose ith entry is given by $h'_i = h_i e^{-j2\pi\nu_i\tau_i}$, and $\mathbf{X}_{P\times MN}$ is the symbol matrix whose ith column ($i = k + Nl$, $i = 0, 1, \cdots, MN-1$) is given by

$$\mathbf{X}[i] = \begin{bmatrix} x_{(k-\beta_1)_N + N(l-\alpha_1)_M} \\ x_{(k-\beta_2)_N + N(l-\alpha_2)_M} \\ \vdots \\ x_{(k-\beta_P)_N + N(l-\alpha_P)_M} \end{bmatrix}$$

(*) G. D. Surabhi, R. M. Augustine, and A. Chockalingam, "On the diversity of uncoded OTFS modulation in doubly-dispersive channels," *IEEE Trans. Wireless Commun.*, vol. 18, no. 6, pp. 3049-3063, Jun. 2019.

Diversity performance of OTFS

- Pairwise error probability (PEP) between $\mathbf{X}_i$ and $\mathbf{X}_j$

$$P(\mathbf{X}_i \to \mathbf{X}_j | \mathbf{h}', \mathbf{X}_i) = Q\left(\sqrt{\frac{\|\mathbf{h}'(\mathbf{X}_i - \mathbf{X}_j)\|^2}{2N_0}}\right)$$

- PEP averaged over the channel statistics can be upper bounded as

$$P(\mathbf{X}_i \to \mathbf{X}_j) \leq \frac{1}{\gamma^r \prod_{l=1}^{r} \frac{\lambda_l^2}{4P}}$$

where λ_l is the lth non-zero singular value of the difference matrix $\mathbf{\Delta}_{ij} = (\mathbf{X}_i - \mathbf{X}_j)$, r is the rank of $\mathbf{\Delta}_{ij}$, and γ is the SNR

- Diversity order

$$\rho_{\text{siso-otfs}} = \min_{i,j \;\, i \neq j} \; \text{rank}(\mathbf{\Delta}_{ij})$$

which is one

Lower bound on BER

- BER can be bounded as

$$\text{BER} \geq \frac{1}{2^{MN}} \sum_{k=1}^{\kappa} P(\mathbf{X}_i \to \mathbf{X}_j),$$

where κ denotes the number of $\mathbf{\Delta}_{ij}$s having rank one

- Assuming BPSK symbols,

$$P(\mathbf{X}_i \to \mathbf{X}_j) = \mathbb{E}\left[Q\left(\sqrt{2\gamma PMN|\tilde{h}_1|^2}\right)\right]$$

- At high SNRs,

$$\text{BER} \geq \frac{\kappa}{2^{MN}} \frac{1}{4\gamma MN}$$

- As the values M and N increase, the 2^{MN} term can dominate the ratio $\dfrac{\kappa}{2^{MN}}$
- BER can decrease with a higher slope for higher frame sizes before meeting the diversity one lower bound

[1] When $P = MN$, $\kappa = 8 \ \forall \ MN$

Diversity results

Simulation parameters:

Parameter	Value
Carrier frequency (GHz)	4
Subcarrier spacing (kHz)	3.75
Number of paths (P)	4
Delay-Doppler profile (τ_i, ν_i)	$(0, 0), (0, \frac{1}{NT}), (\frac{1}{M\Delta f}, 0), (\frac{1}{M\Delta f}, \frac{1}{NT})$
Modulation scheme	BPSK

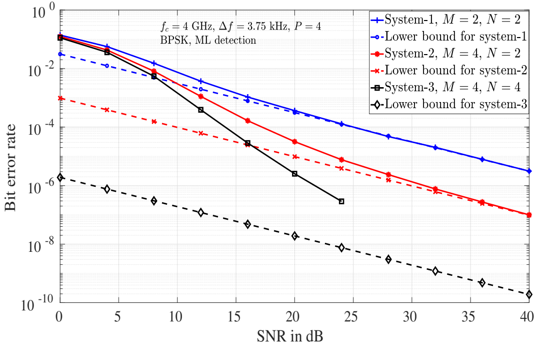

Figure : BER performance of OTFS for $i)$ $M = 2$, $N = 2$, $ii)$ $M = 4$, $N = 2$, $iii)$ $M = 4$, $N = 4$.

Effect of frame size

- Note that the $\frac{\kappa}{2^{MN}}$ values for the considered systems are $\frac{8}{16}$, $\frac{8}{256}$, and $\frac{8}{65536}$, respectively.

- Though the asymptotic diversity order is one, increasing the frame size can lead to higher slopes (> 1) for BER curves in the finite SNR regime.

Choice of M & N

- M decides the delay resolution and $\nu_{\max} < \frac{B}{M} = \Delta f < 1/\tau_{\max}$.
- N decides Doppler resolution and latency ($T_l = NT$).

- Example: For $\tau_{\max} = 1\ \mu$s, $\nu_{\max} = 5$ kHz, $B = 10$ MHz, and $T_l = 1$ ms,
  - $\nu_{\max} < \Delta f < 1/\tau_{\max} \implies 5$ KHz $< \Delta f < 1$ MHz
  - Δf can be chosen to be 20 kHz ($\implies M = \frac{10\times 10^6}{20\times 10^3} = 500$)
  - $T_l = NT = \frac{N}{\Delta f}; \implies N = T_l \Delta f = 1 \times 10^{-3} \times 20 \times 10^3 = 20$
  - (M, N) can be chosen as (500,20)

Phase rotation for full diversity

- Let
$$\mathbf{\Phi} = \mathrm{diag}\left\{\phi_0^{(0)}, \cdots, \phi_{N-1}^{(0)}, \phi_0^{(1)}, \cdots, \phi_{N-1}^{(1)}, \cdots, \phi_{N-1}^{(M-1)}\right\}$$
be the phase rotation matrix and
$$\mathbf{x}' = \mathbf{\Phi}\mathbf{x}$$
be the phase rotated OTFS transmit vector.
- OTFS with the above phase rotation achieves the full diversity of P when $\phi_q^{(l)} = e^{ja_q^{(l)}}$, $q = 0, \cdots, N-1$, $l = 0, \cdots, M-1$ are transcendental numbers with $a_q^{(l)}$ real, distinct, and algebraic.

Full diversity using phase rotation

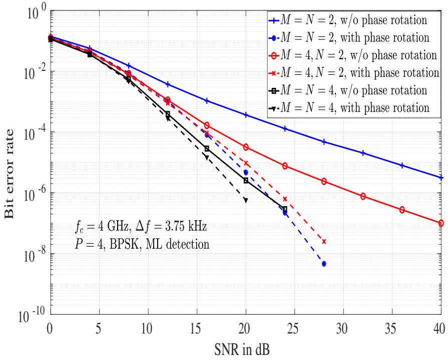

Figure : BER performance of OTFS without and with phase rotation for *i*) $M = N = 2$, *ii*) $M = 4$, $N = 2$, and *iii*) $M = N = 4$, and BPSK.

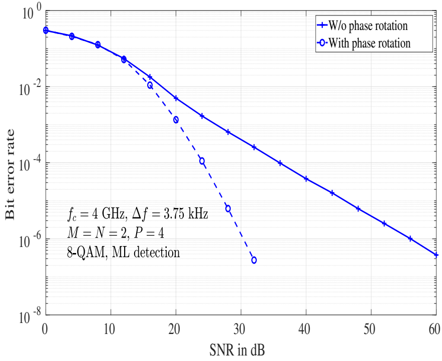

Figure : BER performance of OTFS without and with phase rotation, $M = N = 2$, and 8-QAM.

[1] $\Phi = \text{diag}\{1, e^{j\frac{1}{MN}} \cdots e^{j\frac{MN-1}{MN}}\}$

MIMO-OTFS

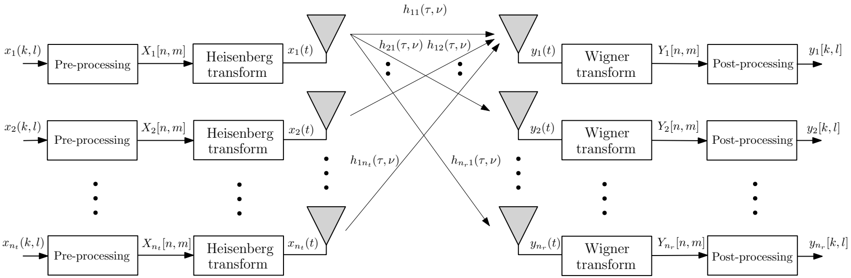

Figure : Block diagram of MIMO-OTFS scheme

- $$\mathbf{y}_{\text{MIMO}} = \mathbf{H}_{\text{MIMO}}\mathbf{x}_{\text{MIMO}} + \mathbf{v}_{\text{MIMO}}$$

(*) M. K. Ramachandran and A. Chockalingam, "MIMO-OTFS in high-Doppler fading channels: Signal detection and channel estimation," *Proc. IEEE GLOBECOM'2018*, Abu Dhabi, UAE, Dec. 2018.

MIMO-OTFS performance

- Delay and Doppler models

Path index (i)	1	2	3	4	5
Delay (τ_i,μs)	2.1	4.2	6.3	8.4	10.4
Doppler (ν_i,Hz)	0	470	940	1410	1880

- Simulation parameters

Parameter	**Value**
Carrier frequency (GHz)	4
Subcarrier spacing (kHz)	15
Frame size (M, N)	$(32, 32)$
Modulation scheme	BPSK
MIMO configuration	1×1, 1×2, 1×3, 2×2, 3×3, 2×3
Maximum speed (kmph)	507.6

MIMO-OTFS performance

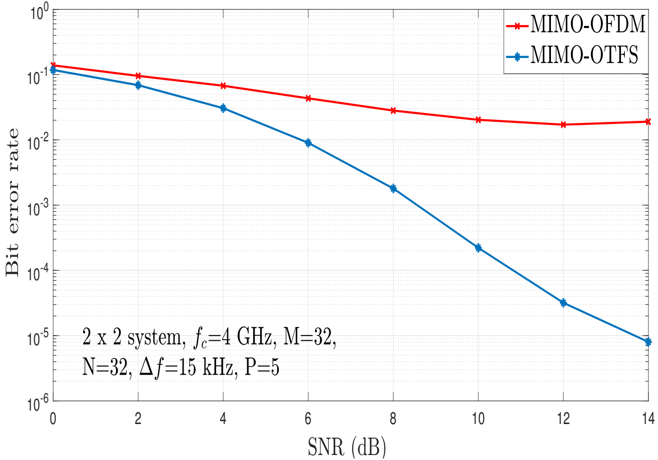

Figure : BER performance comparison between MIMO-OTFS and MIMO-OFDM

Diversity of MIMO-OTFS

- Each row of $\mathbf{H}_{\text{MIMO}}$ has only $n_t P$ non-zero elements and each column has only $n_r P$ non-zero elements. The MIMO-OTFS system model can be written as

$$\begin{bmatrix} \mathbf{y}_1^T \\ \mathbf{y}_2^T \\ \vdots \\ \mathbf{y}_{n_r}^T \end{bmatrix} = \begin{bmatrix} \mathbf{h}'_{11} & \mathbf{h}'_{12} \cdots \mathbf{h}'_{1n_t} \\ \mathbf{h}'_{21} & \mathbf{h}'_{22} \cdots \mathbf{h}'_{2n_t} \\ \vdots & \\ \mathbf{h}'_{n_r 1} & \mathbf{h}'_{n_r 2} \cdots \mathbf{h}'_{n_r n_t} \end{bmatrix} \begin{bmatrix} \mathbf{X}_1 \\ \mathbf{X}_2 \\ \vdots \\ \mathbf{X}_{n_t} \end{bmatrix} + \begin{bmatrix} \mathbf{v}_1^T \\ \mathbf{v}_2^T \\ \vdots \\ \mathbf{v}_{n_r}^T \end{bmatrix},$$

- Diversity order achieved by MIMO-OTFS can be derived as

$$\rho_{\text{mimo-otfs}} = n_r \cdot \min_{i,j \;\; i \neq j, k} \operatorname{rank}(\mathbf{\Delta}_{k,ij}) = n_r$$

- If $MN \times 1$ OTFS transmit vector from each antenna is multiplied by the phase rotation matrix $\mathbf{\Phi}$, then diversity order achieved by phase rotated MIMO-OTFS system is equal to Pn_r

Diversity results in MIMO-OTFS

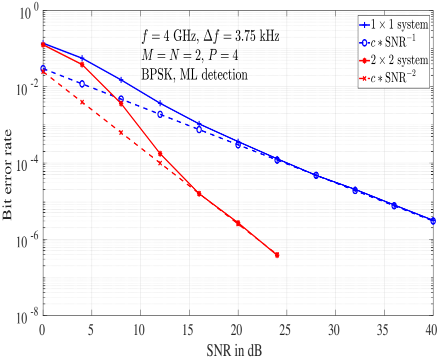

Figure : BER performance of 1×1 SISO-OTFS and 2×2 MIMO-OTFS systems.

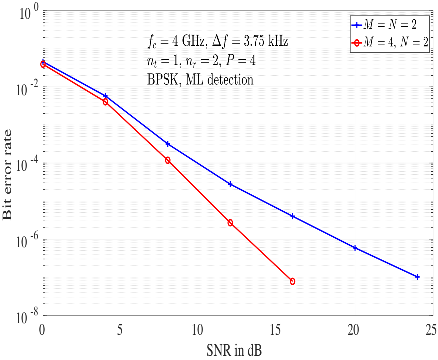

Figure : BER performance of 1×2 OTFS system with $i)$ $M = N = 2$ and $ii)$ $M = 4$, $N = 2$.

Full diversity using phase rotation in MIMO-OTFS

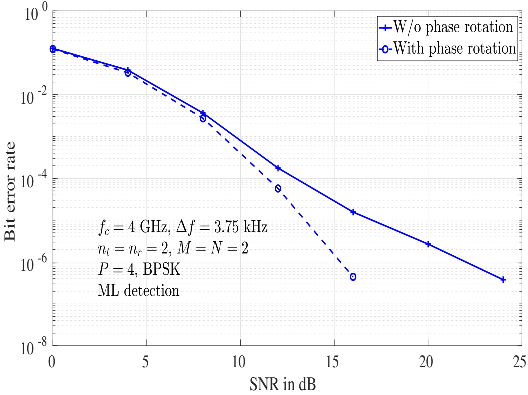

Figure : BER performance of 2×2 MIMO-OTFS system without and with phase rotation, $M = N = 2$.

Space-time coded OTFS

Space-time coded OTFS

- Use of space-time coding in OTFS
- structure of Alamouti code generalized to matrices

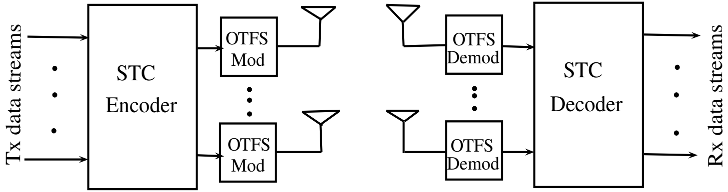

Figure : STC-OTFS scheme.

- Consider the alternate form of input-output relation for SISO-OTFS

$$\mathbf{y}^T = \mathbf{h}'\mathbf{X} + \mathbf{v}^T,$$

where $\mathbf{X}$ is an $MN \times MN$ symbol matrix.

(*) Rose Mary Augustine, G. D.Surabhi and A. Chockalingam, "Space-time coded OTFS modulation in high-Doppler channels," *Proc. IEEE VTC'2019-Spring*, Kuala Lumpur Apr. 2019.

Encoding

- Consider a space-time code (rate-1) using the Alamouti code structure (generalized to matrices)
- quasi-static DD channel over $T'(=2)$ frames

$$\tilde{\mathbf{X}}_{n_t MN \times T' MN} = \tilde{\mathbf{X}}_{2MN \times 2MN} = \begin{bmatrix} \mathbf{X}_1 & -\mathbf{X}_2^H \\ \mathbf{X}_2 & \mathbf{X}_1^H \end{bmatrix}$$

- Corresponding OTFS transmit vectors, $k \in \{1, 2\}$

$$\mathbf{X}_k \Longleftrightarrow \mathbf{x}_k, \quad \mathbf{X}_k^H \Longleftrightarrow (\hat{\mathbf{x}}_k)^* = (\mathbf{P}\mathbf{x}_k)^*.$$

where

$$\mathbf{P} = \mathbf{P}'_M \otimes \mathbf{P}'_N.$$

$$\mathbf{P}'_M = \begin{bmatrix} 1 & 0 & \cdots 0 & 0 \\ 0 & 0 & \cdots 0 & 1 \\ 0 & 0 & \cdots 1 & 0 \\ \vdots & & & \\ 0 & 1 & \cdots 0 & 0 \end{bmatrix}_{M \times M} \mathbf{P}'_N = \begin{bmatrix} 1 & 0 & \cdots 0 & 0 \\ 0 & 0 & \cdots 0 & 1 \\ 0 & 0 & \cdots 1 & 0 \\ \vdots & & & \\ 0 & 1 & \cdots 0 & 0 \end{bmatrix}_{N \times N}.$$

- Transmitted OTFS vectors in the second frame duration are not just the conjugated vectors, but are conjugated and permuted vectors of those transmitted in the first frame duration.

Decoding

- Received vectors in the first and second frame duration are

$$\mathbf{y}_1 = \mathbf{H}_1\mathbf{x}_1 + \mathbf{H}_2\mathbf{x}_2 + \mathbf{v}_1$$
$$\mathbf{y}_2 = -\mathbf{H}_1(\hat{\mathbf{x}}_2)^* + \mathbf{H}_2(\hat{\mathbf{x}}_1)^* + \mathbf{v}_2.$$

- Permutation ($\mathbf{P}$) and conjugation are applied on $\mathbf{y}_2$.

$$\underbrace{\begin{bmatrix} \mathbf{y}_1 \\ (\hat{\mathbf{y}}_2)^* \end{bmatrix}}_{\triangleq\ \bar{\mathbf{y}}} = \underbrace{\begin{bmatrix} \mathbf{H}_1 & \mathbf{H}_2 \\ \mathbf{H}_2^H & -\mathbf{H}_1^H \end{bmatrix}}_{\triangleq\ \bar{\mathbf{H}}} \begin{bmatrix} \mathbf{x}_1 \\ \mathbf{x}_2 \end{bmatrix} + \begin{bmatrix} \mathbf{v}_1 \\ (\hat{\mathbf{v}}_2)^* \end{bmatrix}$$

- Since two block columns of $\bar{\mathbf{H}}$ are orthogonal, the decoding problem for $\mathbf{x}_1$ and $\mathbf{x}_2$ can be decomposed into two separate orthogonal problems.

Diversity

- Let $\tilde{\boldsymbol{\Delta}}_{ij} \triangleq \tilde{\mathbf{X}}_i - \tilde{\mathbf{X}}_j$ be the difference matrix

$$\rho_{\text{STC-OTFS}} = \min\{\min_{i,j\ i\neq j} \text{rank}(\tilde{\boldsymbol{\Delta}}_{ij}), 2P\}.$$

- $\text{rank}(\tilde{\boldsymbol{\Delta}}_{ij})$ can be simplified as

$$\text{rank}(\tilde{\boldsymbol{\Delta}}_{ij}^H \tilde{\boldsymbol{\Delta}}_{ij}) = 2 \times \text{rank}(\boldsymbol{\Delta}_{1,ij}^H \boldsymbol{\Delta}_{1,ij} + \boldsymbol{\Delta}_{2,ij}^H \boldsymbol{\Delta}_{2,ij}).$$

  whose min rank is two.

- STC-OTFS for $2 \times n_r$ can achieve an asymptotic diversity order of $2n_r$.
- With phase rotation applied to each of n_t transmit antennas during every frame duration can yield a full delay Doppler space diversity of $2Pn_r$.

BER performance of STC-OTFS

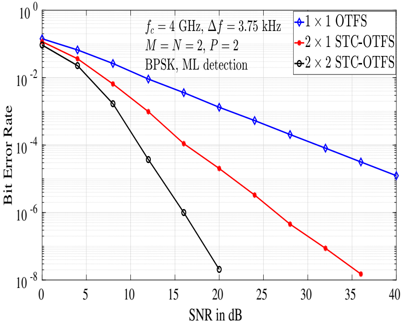

Figure : BER performance of i) 1×1 OTFS, ii) 2×1 STC-OTFS, and iii) 2×2 STC-OTFS for $M = N = 2$.

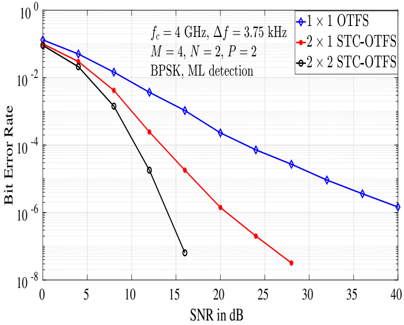

Figure : BER performance of i) 1×1 OTFS, ii) 2×1 STC-OTFS, and iii) 2×2 STC-OTFS for $M = 4, N = 2$.

Phase rotation in STC-OTFS

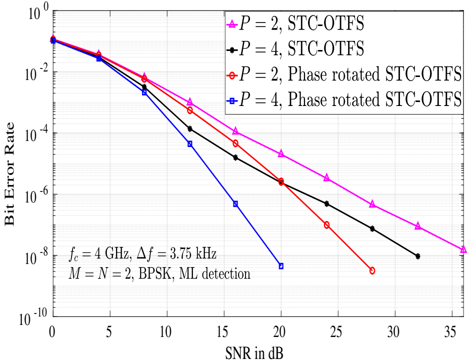

Figure : BER performance of 2×1 STC-OTFS with and without phase rotation for $i)$ $P = 2$ and $ii)$ $P = 4$.

STC-OTFS with phase rotation achieves full spatial and delay-Doppler diversity even for small frame sizes.

PAPR of OTFS

PAPR

- High PAPR is one of the key detrimental aspects in OFDM systems
  - Max. PAPR in OFDM increases with M, no. of subcarriers due to M-point IDFT operation at transmitter

PAPR of OTFS waveform is of interest

- In OTFS, max. PAPR grows linearly with N (and not with M)

(*) G. D. Surabhi, R. M. Augustine and A. Chockalingam, "Peak-to-average power ratio of OTFS modulation," *IEEE Commun. Letters*, vol. 23, no. 6, pp. 999-1002, Jun. 2019.

(**) S. Tiwari and S. S. Das, "Circularly pulse shaped orthogonal time frequency space modulation," arXiv:1910.10457v1 [cs.IT] 23 Oct 2019.

PAPR of OTFS transmit signal

- Time domain OTFS signal is given by

$$s(t) = \sum_{n=0}^{N-1} \sum_{m=0}^{M-1} X[n,m] g_{tx}(t - nT) e^{j2\pi m\Delta f(t-nT)}$$

- Discrete time representation (by Nyquist sampling, $t = (r + qM)T_s$):

$$s(r + qM) = M \sum_{n=0}^{N-1} \tilde{x}_r[n] g_{tx}([r + qM - nM]_{MN})$$

where $\tilde{x}_r[n] = \sum_{k=0}^{N-1} x[k,r] e^{\frac{j2\pi nk}{N}}$ (nth IDFT), $r = 0, \cdots, M-1$ and $q = 0, \cdots, N-1$

Upper bound on PAPR

$$\mathrm{PAPR} = \frac{\max\limits_{r,q}\{|s(r+qM)|^2\}}{P_{\mathrm{avg}}},$$

where

$$P_{\mathrm{avg}} = \frac{M^2 N \sigma_a^2}{MN} \sum_{n=0}^{N-1} \sum_{r=0}^{M-1} \sum_{q=0}^{N-1} |g_{tx}([r+qM-nM]_{MN})|^2$$

$$\max_{r,q} |s(r+qM)|^2 \leq M^2 N^2 \max_{k,l} |x[k,l]|^2 \max_{r,q} \sum_{n=0}^{N-1} |g_{tx}([r+qM-nM]_{MN})|^2$$

For rectangular pulse,

$$\mathrm{PAPR}_{\mathrm{max}} = \frac{N \max\limits_{c\in\mathbb{A}} |c|^2}{\sigma_a^2}$$

$\mathrm{PAPR}_{\mathrm{max}}$ grows linearly with N and not with M.

CCDF of PAPR

- Time domain samples of the OTFS transmit signal with rectangular pulse are the N-point IDFT values of the DD symbols along Doppler domain.
- If N is large, then by CLT, the transmitted samples can be approximated to have complex Gaussian distribution with zero mean.
- CCDF of PAPR can be derived as

$$P\left(\text{PAPR} > \gamma_0\right) \approx 1 - \left(1 - e^{-\gamma_0}\right)^{MN}$$

PAPR performance of OTFS

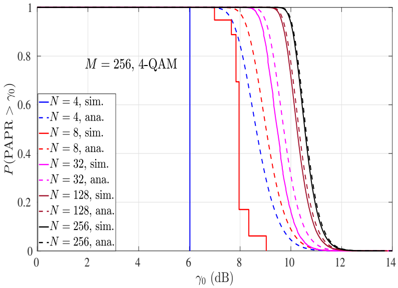

Figure : Analytical and simulated CCDF of PAPR in OTFS.

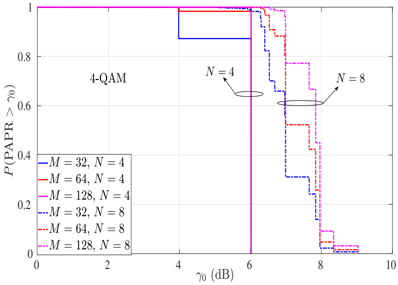

Figure : Effect of M and N on the CCDF of PAPR in OTFS.

PAPR of OTFS, OFDM and GFDM

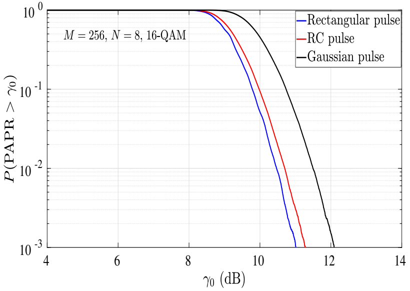

Figure : CCDF of the PAPR of OTFS for different pulse shapes.

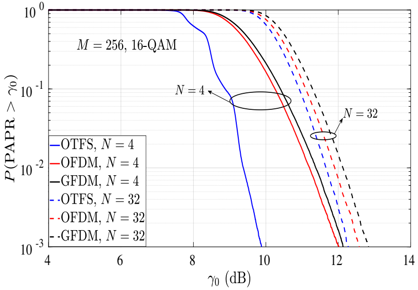

Figure : Comparison of CCDF of the PAPR of OTFS with those of OFDM and GFDM with 16-QAM.

OTFS can have better PAPR compared to OFDM and GFDM when $N < M$.

Channel estimation in OTFS

Channel estimation in the delay-Doppler domain

- Each tx and rx antenna pair sees a different channel having a finite support in the delay-Doppler domain
- The support is determined by the delay and Doppler spread of the channel
- Input-output relation for pth tx and qth rx antenna pair can be written as

$$\hat{x}_q[k,l] = \sum_{m=0}^{M-1} \sum_{n=0}^{N-1} x_p[n,m] \frac{1}{MN} h_{w_{qp}} \left(\frac{k-n}{NT}, \frac{l-m}{M\Delta f} \right) + v_q[k,l]$$

- Transmit pilot from pth antenna

$$\begin{aligned} x_p[n,m] &= 1 \text{ if } (n,m) = (n_p, m_p) \\ &= 0 \ \forall\ (n,m) \neq (n_p, m_p) \end{aligned}$$

- Received signal at the qth rx antenna will be

$$\hat{x}_q[k,l] = \frac{1}{MN} h_{w_{qp}} \left(\frac{k-n_p}{NT}, \frac{l-m_p}{M\Delta f} \right) + v_q[k,l]$$

- $\frac{1}{MN} h_{w_{qp}} \left(\frac{k}{NT}, \frac{l}{M\Delta f} \right)$ and thus $\hat{\mathbf{H}}_{qp}$ can be estimated, since n_p and m_p are known at the receiver a priori

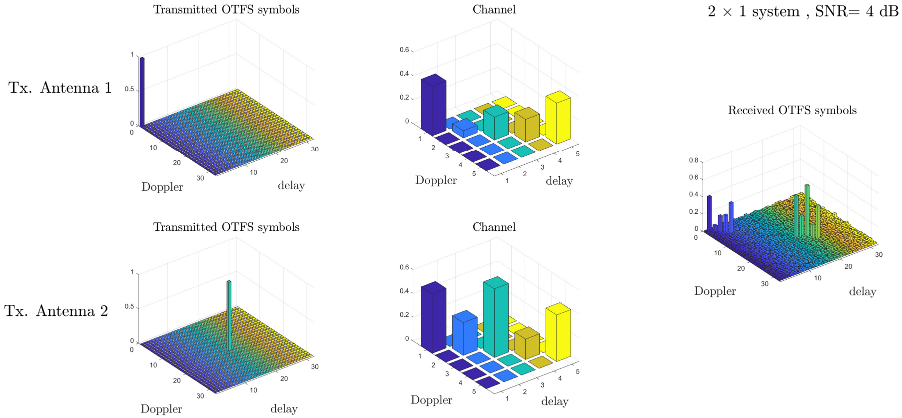

Figure : Illustration of pilots and channel response in delay-Doppler domain in a 2×1 MIMO-OTFS system

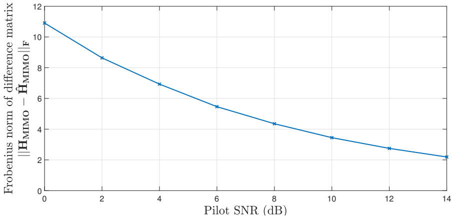

Figure : Frobenius norm of the difference matrix $\mathbf{H}_{\text{MIMO}} - \hat{\mathbf{H}}_{\text{MIMO}}$ as a function of pilot SNR in a 2×2 MIMO-OTFS system

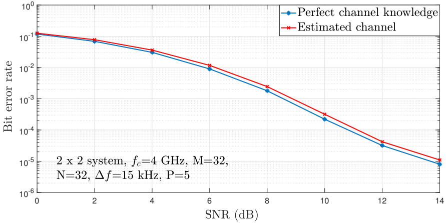

Figure : BER performance of 2×2 MIMO-OTFS system using the estimated channel

Multiuser OTFS (OTFS-MA)

Multiuser OTFS

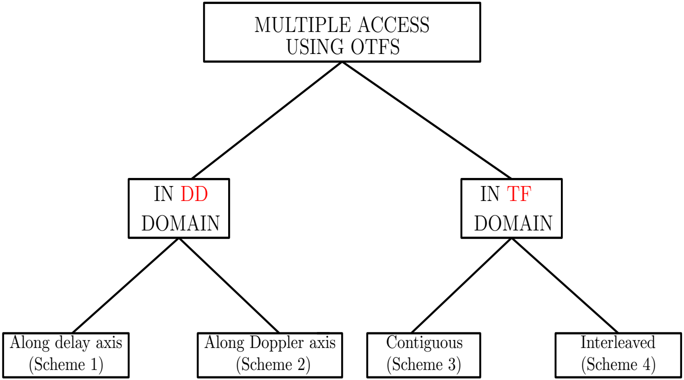

(*) G. D. Surabhi, R. M. Augustine, and A. Chockalingam, "Multiple access in the delay-Doppler domain using OTFS modulation," *ITA'2019*, San Diego, Feb. 2019. Online: arXiv:1902.03415 [sc.IT] 9 Feb 2019.

(**) V. Khammammetti and S. K. Mohammed, "OTFS based multiple-access in high Doppler and delay spread wireless channels," *IEEE Wireless Commun. Lett.*, doi: 10.1109/LWC.2018.2878740.

(***) R. M. Augustine and A. Chockalingam, "Interleaved time-frequency multiple access using OTFS modulation," *IEEE VTC2019-Fall*, Honolulu, Sep. 2019.

OTFS-MA in the delay-Doppler domain

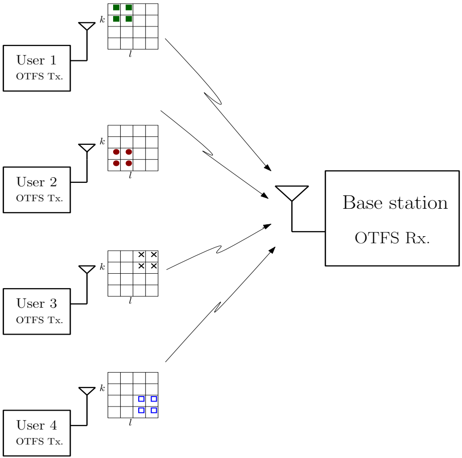

Figure : OTFS multiple access (OTFS-MA) on the uplink

- Bins in the delay-Doppler grid Γ serve as the delay-Doppler resource blocks (DDRBs)
- Different DDRBs are allocated to different users for multiple access
- Denoting the OTFS symbol vector transmitted by uth user by $\mathbf{x}_u \in \mathbb{C}^{MN \times 1}$

$$\mathbf{y} = \sum_{u=0}^{K_u - 1} \mathbf{H}_u \mathbf{x}_u + \mathbf{v}$$

DDRB allocation schemes

Scheme 1- Multiplexing along delay axis

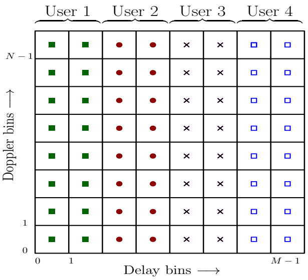

Figure : DDRB allocation in an $N \times M$ delay-Doppler grid in Scheme 1.

Scheme 2- Multiplexing along Doppler axis

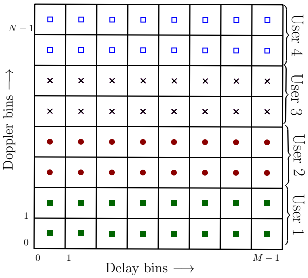

Figure : DDRB allocation in an $N \times M$ delay-Doppler grid in Scheme 2.

The 2D circular convolution operation with channel results in each user's symbols to experience MUI, requiring the BS to jointly decode the symbols.

DDRB allocation schemes

Scheme 3 - MUI-free allocation

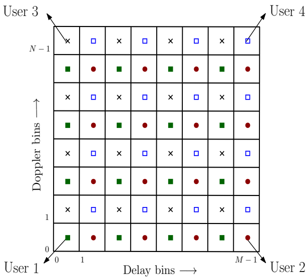

Figure : DDRB allocation in an $N \times M$ delay-Doppler grid in Scheme 3 .

- MN/K_u symbols from a given user are placed at equal intervals in the delay as well as Doppler domains (g_1 and g_2 respectively where $K_u = g_1 g_2$) .
- $X_u[n, m]$ can be restricted to a region $[\frac{NT}{g_2}(u)_{g_2}, \frac{NT}{g_2}((u)_{g_2}+1)]$ in time and $[\frac{M}{g_1}\lfloor u/g_2 \rfloor \Delta f, \frac{M}{g_1}(\lfloor u/g_2 \rfloor + 1)\Delta f]$ in frequency.
- Reduced detection complexity.

[1] V. Khammammetti, S. K. Mohammed, "OTFS based multiple-access in high Doppler and delay spread wireless channels," *IEEE Wireless Commun. Lett.* vol. 8, pp. 528-531, Apr. 2019.

OTFS-MA performance

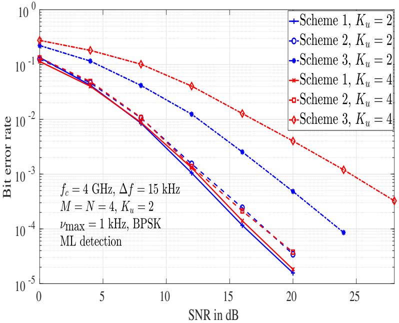

Figure : BER performance of uplink OTFS-MA with different DDRB allocation schemes with $M = N = 4$, $K_u = 2, 4$, and ML detection [1].

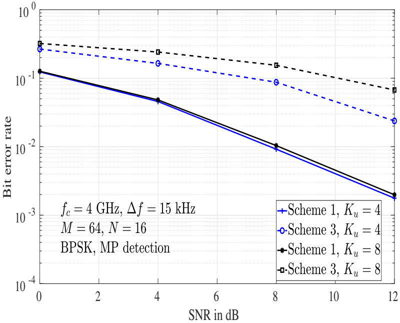

Figure : BER performance of uplink OTFS-MA with DDRB allocation Schemes 1 and 3 with $K_u = 4, 8$ users, $M = 64$, $N = 16$, and MP detection[2]

[1] 4 tap channel, $\tau_{u,i} = \{0, 16.6, 33.3, 50\}\mu s$, $\nu_{\max} = 1$ KHz $\forall u$

[2] 10 tap channel, $\tau_{u,i} = \{0,\ 1.04,\ 2.08,\ 3.12,\ 4.16,\ 5.2,\ 6.25,\ 7.29,\ 8.33,\ 9.37\}\ \mu s$, $\nu_{\max} = 1$ KHz $\forall\ u$.

OTFS-MA Vs SC-FDMA and OFDMA

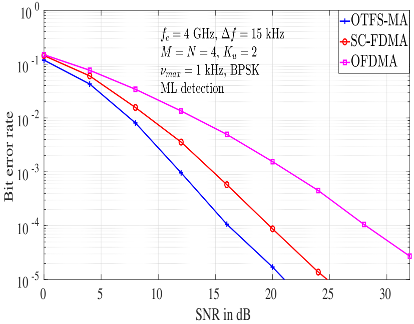

Figure : BER performance comparison between OTFS-MA, OFDMA, and SC-FDMA with ML detection.

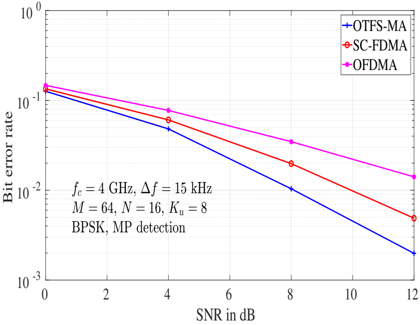

Figure : BER performance comparison between OTFS-MA, OFDMA, and SC-FDMA with MP detection.

- OTFS-MA achieves better performance compared to OFDMA and SC-FDMA on the uplink.

OTFS with phase noise

OTFS with phase noise

- Phase noise spectrum

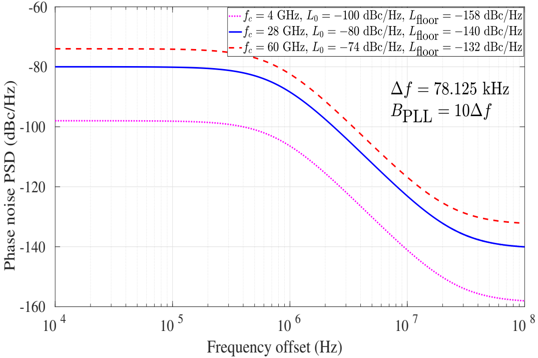

Figure : PSD of oscillator phase noise for various carrier frequencies (4 GHz, 28 GHz, 60 GHz).

$$L(f_m) = \frac{B_{\text{PLL}}^2 L_0}{B_{\text{PLL}}^2 + f_m^2} + L_{\text{floor}}$$

(*) G. D. Surabhi, M. K. Ramachandran, and A. Chockalingam, "OTFS modulation with phase noise in mmWave communications," *Proc. IEEE VTC'2019-Spring*, Kuala Lumpur, Apr. 2019.

PLL bandwidth and variance of phase noise

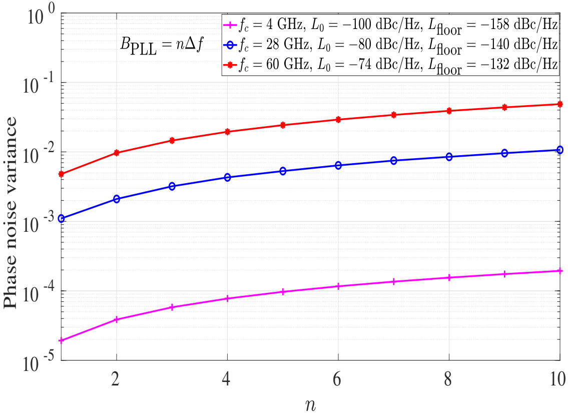

Figure : Variance of the oscillator phase noise as a function of n where $B_{\text{PLL}} = n\Delta f$.

Simulation parameters

Parameter	**Value**
Carrier frequency (GHz)	28
Bandwidth (MHz)	10
Subcarrier spacing, Δf (kHz)	78.125
Frame size (M, N)	(128,64)
Modulation	BPSK
No. of taps, P	5
Delay profile (μs)	0.3, 1, 1.7, 2.4, 3.1
Doppler profile (Hz)	0, -400, 400, -1220, 1220

BER performance

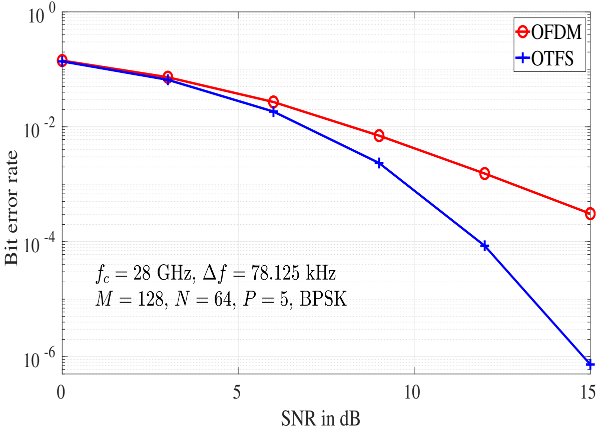

Figure : BER performance comparison between OTFS and OFDM systems with phase noise and Doppler shifts.

Conclusions

- OTFS modulation
  - an emerging and promising modulation scheme for high-Doppler fading channels
  - multiplexing in the delay-Doppler domain
  - impressive performance (superior performance compared to OFDM)
  - implementation using pre- and post-processing blocks to OFDM
  - simple channel estimation in the delay-Doppler domain
  - can serve in interesting use cases (high-speed trains, autonomous vehicles, drones, mmWave communications)
  - Promising modulation scheme for 5G and beyond

Publications from our group

- G. D. Surabhi and A. Chockalingam, “Low-complexity Linear Equalization for OTFS modulation,” *IEEE Commun. Letters*, Nov. 2019.
- G. D. Surabhi, R. M. Augustine, and A. Chockalingam, “On the diversity of uncoded OTFS modulation in doubly-dispersive channels,” *IEEE Trans. Wireless Commun.*, vol. 18, no. 6, pp. 3049-3063, Jun. 2019.
- G. D. Surabhi, R. M. Augustine and A. Chockalingam, “Peak-to-average power ratio of OTFS modulation,” *IEEE Commun. Letters*, vol. 23, no. 6, pp. 999-1002, Jun. 2019.
- R. M. Augustine and A. Chockalingam, “Interleaved time-frequency multiple access using OTFS modulation,” *IEEE VTC2019-Fall*, Honolulu, Sep. 2019.
- G. D. Surabhi, R. M. Augustine, and A. Chockalingam, “Multiple access in the delay-Doppler domain using OTFS modulation,” *ITA'2019*, San Diego, Feb. 2019. Online: arXiv:1902.03415 [sc.IT] 9 Feb 2019.
- Rose Mary Augustine, G. D.Surabhi and A. Chockalingam, “Space-time coded OTFS modulation in high-Doppler channels,” *Proc. IEEE VTC'2019-Spring*, Kuala Lumpur Apr. 2019.
- G. D. Surabhi, M. K. Ramachandran, and A. Chockalingam, “OTFS modulation with phase noise in mmWave communications,” *Proc. IEEE VTC'2019-Spring*, Kuala Lumpur Apr. 2019.
- M. K. Ramachandran and A. Chockalingam, “MIMO-OTFS in high-Doppler fading channels: Signal detection and channel estimation,” *Proc. IEEE GLOBECOM'2018*, Abu Dhabi, UAE, Dec. 2018. Online: arXiv:1805.02209 [cs.IT] 6 May 2018.
- K. R. Murali and A. Chockalingam, “On OTFS modulation for high-Doppler fading channels,” *ITA'2018*, San Diego, Feb. 2018. Online: arXiv:1802.00929 [cs.IT] 3 Feb 2018.

Thank you